Chapter 4

Studies on Heterogeneous Pd-Based Catalytic System for C–H Bond Functionalization at C2 Position of Indoles

This chapter is composed of two sections delivering two different heterogeneous Pd-based catalytic systems for directing-group-free C2-arylation of indoles with arylboronic acids.

Section A

Palladium-on-Carbon as a Reusable Heterogeneous Catalyst for C2-Arylation of N-Alkylated Indoles with Arylboronic Acids

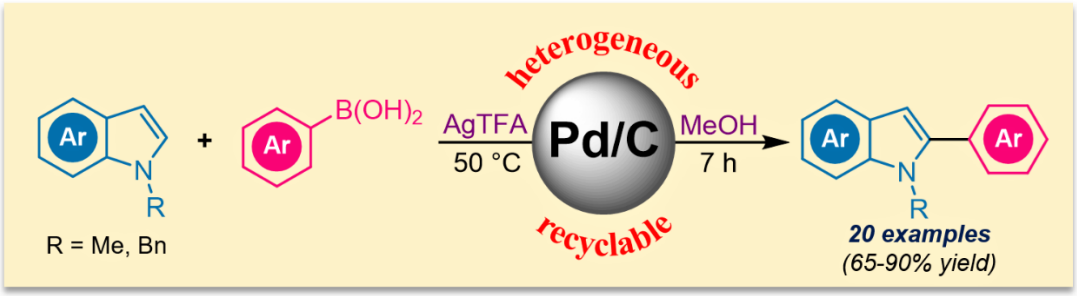

4A.1 Introduction

Transition metal catalyzed C–H activation has emerged as an influential means for the direct functionalization of inactivated C–H bonds empowering previously impossible transformations, directing new selectivity, and shortened reaction paths [1-3]. Various coupling partners have been employed in the arena of C–H arylation of indoles and pyrroles using aryl halides [4-6], hypervalent iodine electrophiles [7-9], and arylsiloxanes [10,11]. Despite significant advantages, there occurs certain limitations such as high reaction temperature, acidic medium, long reaction times, use of ligands and directing groups [12-15]. Compared to other coupling partners, organoboronates exhibits some unique advantages including non-toxicity, high stability, environment-friendly and ease of availability [16,17]. Therefore, development of mild and efficient methods for regioselective direct C–H arylation of indoles demands extensive research.

In the present juncture, a plethora of methodologies have been reported for the transition metal-mediated selective C2-arylation of indole with organoborane reagents, with Pd [18,19], Rh [20,21], Ru [22,23], Cu [24,25], Co [26] based catalytic systems. However, most of these reported methods, demand the use of acidic solvents [27], high reaction temperature [22], and expensive metal catalysts in homogeneous form causing difficulty in their separation and recovery, thus causing environmental and economic concerns. In contrast heterogeneous catalysts provide ease of separation and possibility of catalyst recyclability. Till date, only few literatures have been available for direct C–H arylation of indoles using heterogeneous Pd catalysts [28-34].

In this context, palladium-on-carbon (Pd/C) can offer as a beneficial alternative to conventional homogeneous catalysis for C–H arylation of indoles [35]. Compared to other expensive and air-sensitive Pd catalysts, Pd/C exhibits suitable properties being commercially available, ease of handling, easy recovery, and reusability [36]. It has been successfully employed as a catalyst in various organic transformations [37]. Inspired by these reports, this section describes a Pd/C catalyzed methodology for C2-arylation of indoles with arylboronic acids in absence of any ligands or directing groups (Scheme **4A.1**).

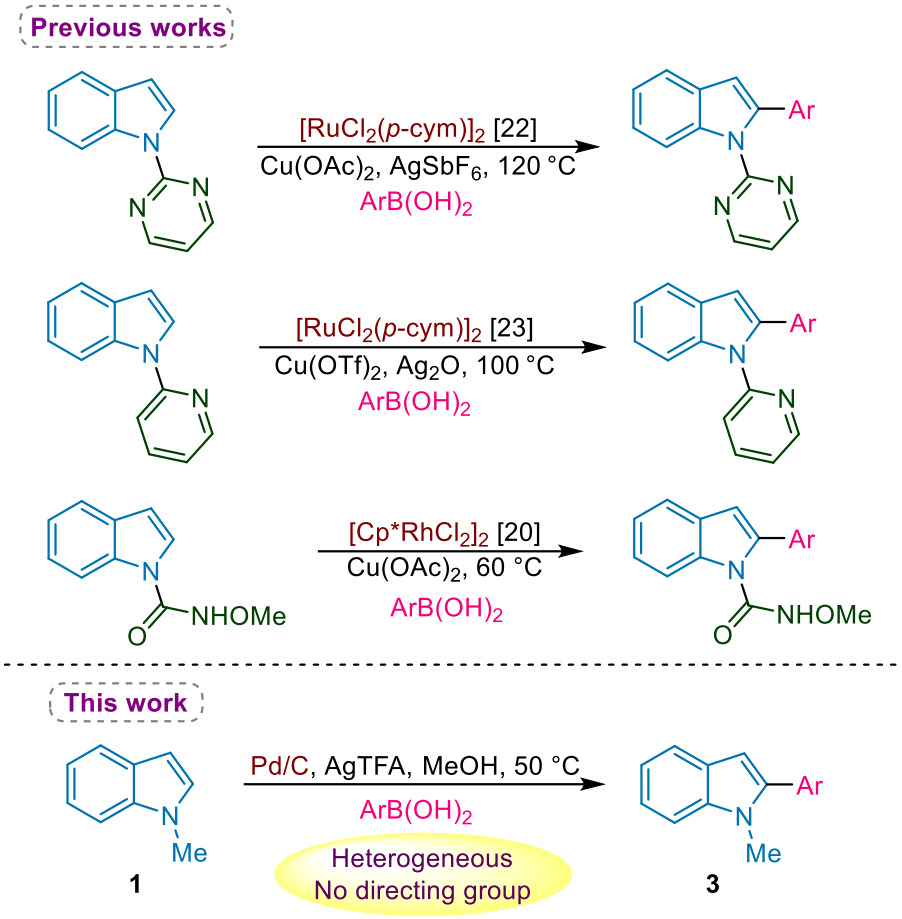

Scheme 4A.1 Previous and present study on direct C–H arylation of indoles

4A.2 Results and Discussion

4A.2.1 Optimization of Reaction Conditions

C–H arylation of 1-methylindole (**1a**) with phenylboronic acid (**2a**) was chosen as the model reaction and the optimization is outlined in Table **4A.1**. In presence of 10% Pd/C (5 mol%) and AgTFA (0.4 mmol), the desired product is obtained in 86% yield (Table **4A.1**, entry **2**). However, no product formation was observed in the absence of an oxidant (Table **4A.1**, entry **1**). Encouraged by the results, a variety of copper and silver salts have been verified as oxidants in the catalytic system and the results are summarized. Copper salts such as $Cu(OAc)_2 \cdot H_2O$ and $Cu(OTf)_2$ and silver salts such as Ag_2O, Ag_2CO_3, AgBr, $AgNO_3$ remain almost ineffective for the transformation (Table **4A.1**, entries **3-8**) while AgOAc produced 40% of the reaction product (Table **4A.1**, entry **9**). Even combination of Cu-Ag salts remained inactive for the current reaction (Table **4A.1**, entry **10**).

Table 4A.1 Screening of reaction conditions for C2-arylation of indoles[a]

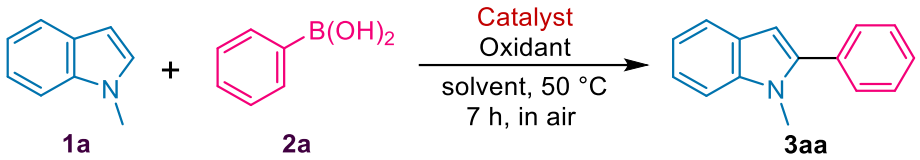

Entry	Catalyst	Oxidant	Solvent	Yield (%)[b] of **3aa**
1	10% Pd/C	-	MeOH	nr
2	10% Pd/C	AgTFA	MeOH	86
3	10% Pd/C	$Cu(OAc)_2{\cdot}H_2O$	MeOH	nr
4	10% Pd/C	$Cu(OTf)_2$	MeOH	20
5	10% Pd/C	Ag_2O	MeOH	nr
6	10% Pd/C	Ag_2CO_3	MeOH	nr
7	10% Pd/C	AgBr	MeOH	nr
8	10% Pd/C	$AgNO_3$	MeOH	nr
9	10% Pd/C	AgOAc	MeOH	40
10	$Cu(OAc)_2{\cdot}H_2O$	AgTFA	MeOH	nr
11	$Pd(OAc)_2$	AgTFA	MeOH	84
12	$NiCl_2{\cdot}6H_2O$	AgTFA	MeOH	30
13	$Co(NO_3){\cdot}6H_2O$	$AgNO_3$	MeOH	trace
14[c]	$Ni(OAc)_2{\cdot}4H_2O$	AgTFA	DMF	50
15	Rh/C	AgTFA	MeOH	nr
16[d]	10% Pd/C	AgTFA	MeOH	72
17[e]	10% Pd/C	AgTFA	MeOH	66
18[f]	10% Pd/C	AgTFA	MeOH	86
19[g]	10% Pd/C	AgTFA	MeOH	63
20[h]	10% Pd/C	AgTFA,	MeOH	trace
21	10% Pd/C	AgTFA	EtOH	75
22	10% Pd/C	AgTFA	*i*-PrOH	68
23	10% Pd/C	AgTFA	*t*-BuOH	27
24	10% Pd/C	AgTFA	CH_3CN	nr
25	10% Pd/C	AgTFA	THF	10
26	10% Pd/C	AgTFA	H_2O	nr

27	10% Pd/C	AgTFA	DMSO	60
28	10% Pd/C	AgTFA	DMF	65

[a]Reaction conditions: **1a** (1 mmol), **2a** (1.2 mmol), catalyst (5 mol%), oxidant (0.4 mmol), solvent (1 mL), T (50 °C), time (7 h), in air; [b]isolated yield; [c]1,10-phen (10 mol%), T (100 °C); [d]T (40 °C); [e]catalyst (2 mol%); [f]catalyst (10 mol%); [g]N_2 atmosphere; [h]K_2CO_3 (3 equiv), 90% yield of biphenyl; nr (no reaction).

A variety of metal catalysts have been investigated such as $Pd(OAc)_2$ which obtained the desired product in 84% yield (Table **4A.1**, entry **11**) whereas $NiCl_2{\cdot}6H_2O$, $Co(NO_3){\cdot}6H_2O$, $Ni(OAc)_2{\cdot}4H_2O$, Rh/C attained lower reaction yields (Table **4A.1**, entries **12-15**). In order to study the effect of temperature, reactions were performed at 40 °C and 50 °C and the better result was observed at 50 °C (Table **4A.1**, entries **2, 16**). For studying the effectiveness of Pd/C as catalyst, reactions were performed varying the amount of the catalyst. Use of 2 mol% of the catalyst gave lower yield (Table **4A.1**, entry **17)** and increased amount of catalyst to 10 mol% gave no significant improvement in the yield (Table **4A.1**, entry **18**). Thus, the highest activity is observed using 5 mol% of the catalyst (Table **4A.1**, entry **2**). However, performing the reaction under N_2 atmosphere produced a relatively lower yield of 63% (Table **4A.1**, entry **19**), which signifies the role of aerial oxidizing environment in the reaction. Effect of base was also studied for the current protocol, but resulted in complete self-coupling of arylboronic acids to corresponding biaryls in 90% yield and no trace of arylation at indole was observed (Table **4A.1**, entry **20**). A variety of solvent media have been investigated for the current protocol. Protic solvents such as EtOH, *i*-PrOH and *t*-BuOH produced moderate yields (Table **4A.1**, entries **21-23**) whereas other solvents such as CH_3CN, THF, H_2O, remained ineffective for the transformation (Table **4A.1**, entries **24-26)** except for DMSO and DMF which formed 60-65% yield of products (Table **4A.1**, entry **27-28**). The methodology did not necessitate the presence of any directing groups or ligands to achieve C2 selectivity.

4A.2.2 Substrate Scope Study

With the optimized reaction condition, the scope and limitations of the C2-arylation of indoles were explored based on electronically varied indole and arylboronic acid derivatives as represented in Table **4A.2**.

Table 4A.2 Substrate scope for C2-arylation of indoles with arylboronic acids[a]

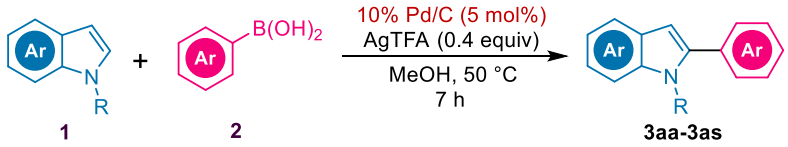

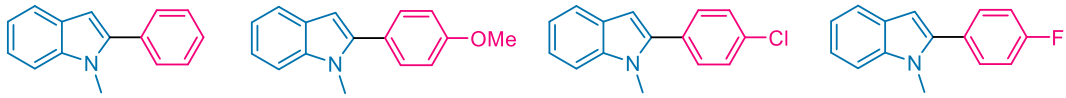

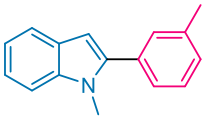

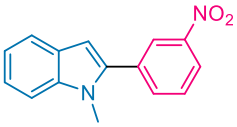

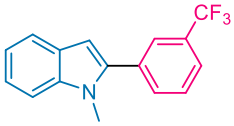

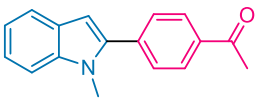

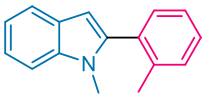

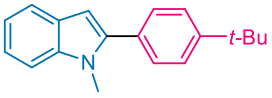

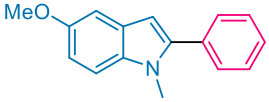

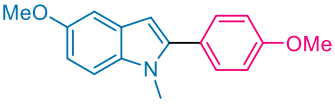

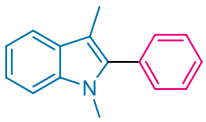

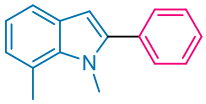

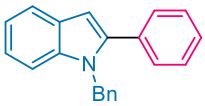

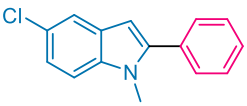

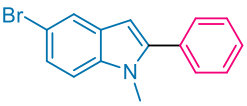

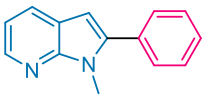

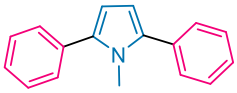

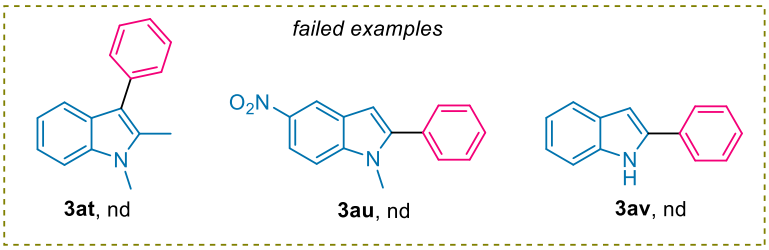

[a]Reaction conditions: **1** (1 mmol), **2** (1.2 mmol), catalyst (5 mol%), AgTFA (0.4 mmol), solvent (1 mL), T (50 °C), time (7 h), in air; the yields reported are the isolated yields; nd (not detected).

A range of phenylboronic acids participated in the regioselective arylation of 1-methylindole and produced the C2-arylated products selectively. The reaction tolerates both electron-donating substituents such as OMe, Me, *t*-Bu (Table **4A.2**,

3ab, 3ae, 3ai-3aj) and electron-withdrawing substituents such as Cl, F, NO_2, CF_3, COMe (Table **4A.2**, **3ac-3ad, 3af-3ah**) irrespective of their positions whether *ortho*, *meta* or *para*, produced acceptable yields of the C2-arylated products (70-88%). These results indicate no correlation between the reaction yield and the electronic nature of arylboronic acid substituents. However, the electronic nature of the indole nucleus plays a vital role in the reaction. Both 1-methylindole and 1-benzylindole gave high yield and selectivity of the C2-arylated products (Table **4A.2**, **3aa, 3ao**). Conversely, free *N*–H indole remained unreactive for the arylation (Table **4A.2**, **3av**). Substituent groups on the indole influenced the reactivity of direct arylation reaction. Electron-rich substituents on indole such as OMe, Me showed better reactivity and afforded the selective arylation product in good yields (82-88% yields) irrespective of position (Table **4A.2**, **3ak-3an**) compared to electron-poor substituents on indole such as Cl, Br which furnished about 65-68% of desired product (Table **4A.2**, **3ap-3aq**) and NO_2 group remained inert to the transformation (Table **4A.2**, **3au**). Interestingly, replacing the benzene ring of 1-methylindole with pyridine did not perturb the reactivity and afforded the direct arylation product in 71% yield (Table **4A.2**, **3ar**). Sterically demanding 1,3-dimethylindole reacted smoothly and afforded 82% of the desired product (Table **4A.2**, **3am**) whereas 1**,**2-dimethylindole resulted in no feasible conversion (Table **4A.2**, **3at**). Also, 1-methylpyrrole produced 2,5-diarylated product arylating both the positions adjacent to nitrogen (Table **4A.2**, **3as**).

In reactions involving immobilized palladium catalyst where the catalyst acts as reservoir of Pd species it is important to elucidate the behaviour of Pd/C catalyst in the current arylation reaction. Following experiments were performed to recognize the behaviour of palladium catalysis.

4A.2.3 Hot-Filtration Test

Hot-filtration test is performed to verify the heterogeneity of the catalyst. A round bottom flask is charged with 10% Pd/C (5 mol%, 5.3 mg) and AgTFA (0.4 mmol, 80 mg) in MeOH (1 mL) at 50 °C. After 4h, the solid catalyst phase was filtered-off using a Whatman filter paper (grade 41) at the reaction temperature. The filtrate was collected in another round bottom flask and **1a** (1 mmol) and **2a** (1.2 mmol) were

added. After 24 h, trace amount of product formation is detected. The ICP-OES analysis of the liquid phase reveals residual Pd level of less than 0.01 ppm. This suggests the heterogeneous nature of the active catalyst species.

4A.2.4 Reusability test

Reusability is an important aspect for any heterogeneous catalyst. In the current system, the Pd catalyst was recycled for four cycles with the model substrates **1a** and **2a** (Figure **4A.1**).

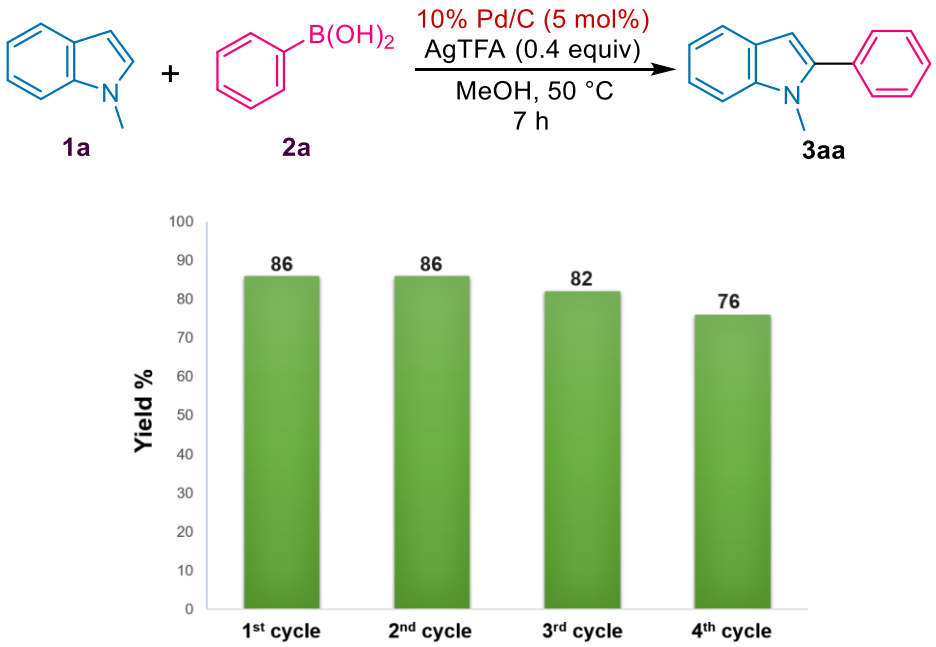

Figure 4A.1 Reusability of Pd/C over four cycles

After the first catalytic cycle, the product **3aa** was isolated by extraction with ethyl acetate and the catalyst species was recovered by centrifugation for the next catalytic run. The recovered residue was washed with water and ethyl acetate and used without further modification followed by addition of fresh reactants for the consecutive cycle. Identical results were obtained up to 2nd cycle, thereafter a slight loss in activity was observed in 3rd and 4th cycles. The observed loss in reactivity over the repeated use is probably due to physical loss of the catalyst.

4A.2.5 Characterization of Recovered Catalyst

The chemical bonding information and oxidation state of catalyst recovered after the 4th cycle is examined by X-ray photoelectron spectroscopy (XPS) analysis.

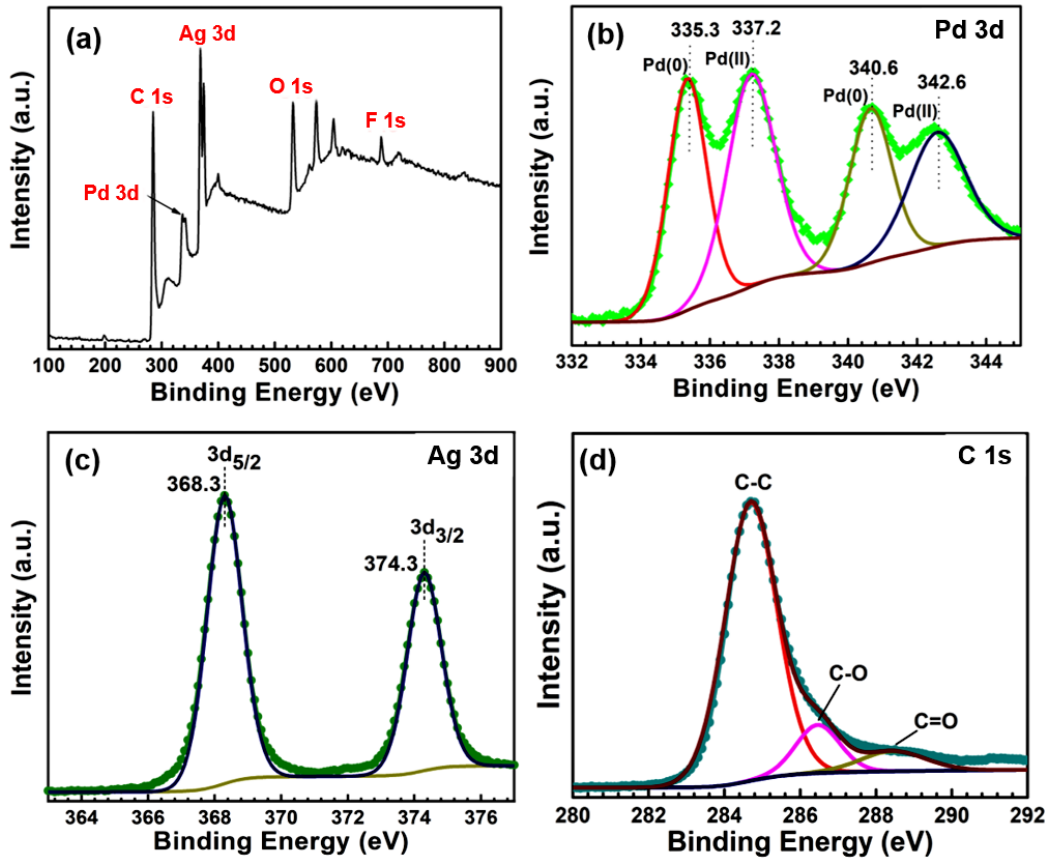

Figure 4A.2 (a) Survey scans XPS spectrum of the reused catalyst, and corresponding high resolution deconvoluted XPS spectra of (b) Pd 3d, (c) Ag 3d, and (d) C 1s

The survey scans XPS spectrum of the reused sample is shown in **Figure 4A.2a**, which comprises five different sharp peaks at binding energies of 284.8 eV, 336.9 eV, 368.1 eV, 532.2 eV, and 688.7 eV signifying the presence of C, Pd, Ag, O, and F respectively. The high-resolution deconvoluted Pd 3d spectra show peaks at binding energies of 335.3 eV and 340.6 eV indicating the presence of Pd(0) species (**Figure 4A.2b**) [38]. Similarly, two peaks of high-resolution Pd 3d spectra at binding energies of 337.2 eV and 342.6 eV corresponds to the Pd(II) species [38]. The high-resolution Ag 3d spectrum is obtained with two binding energy peaks at 368.3 eV and 374.3 eV assigned as the spin-orbit splitting of $Ag3d_{5/2}$ and $Ag3d_{3/2}$ respectively, which specify the metallic nature of Ag in the reused sample (**Figure 4A.2c**) [39]. The detection of Ag(0) particles in the reused sample signifies the role of AgTFA as the oxidant in the reaction, thus itself getting reduced in the process. Also, the presence of Pd(II) might be attributed to the oxidation of Pd(0) species to Pd(II) in presence of the oxidant. Further, the high-resolution C1s spectrum fitted with three different binding energies

peaks at 284.7 eV, 286.7 eV, and 288.4 eV belong to the C–C, C–O, and C=O bonds of TFA, respectively (**Figure 4A.2d**).

4A.2.6 Plausible Mechanism

From the experimental observations and literature findings, a plausible mechanism has been proposed as shown in the **Scheme 4A.2**.

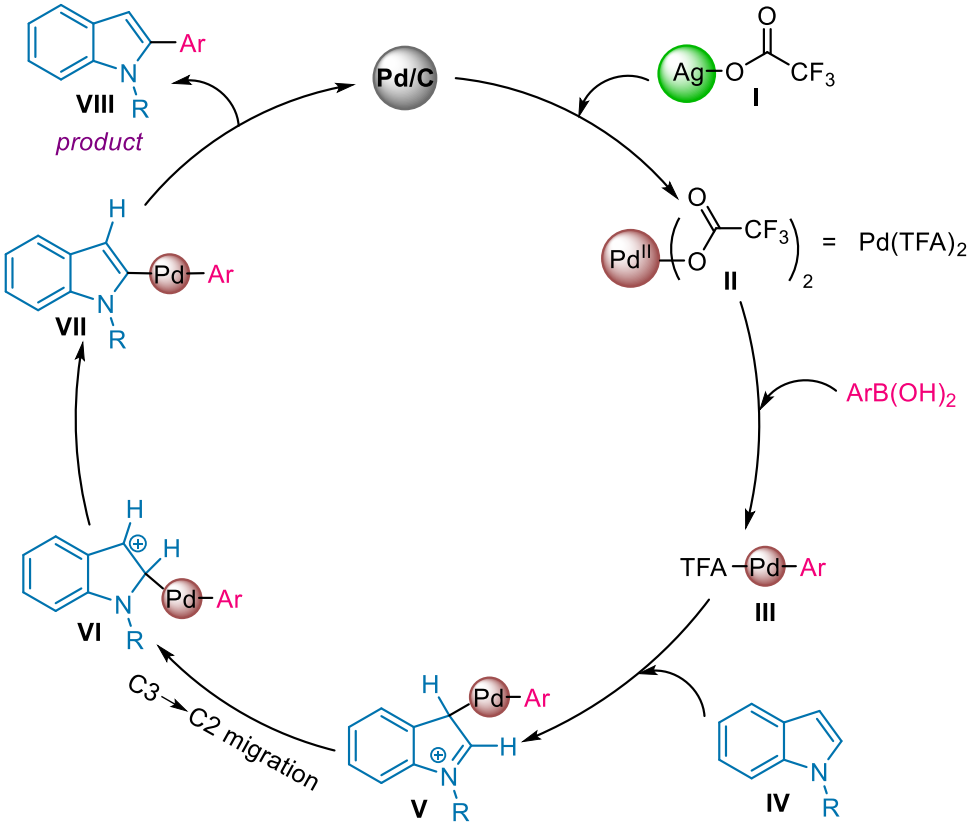

Scheme 4A.2 Plausible mechanism for C2-arylation of indoles

The first step is expected to be the generation of active Pd(II) species (**II**) from Pd(0) deposited on the surface of charcoal by the silver oxidant [40,41]. Initially, arylboronic acid is activated by the Pd(II) species forming the palladium intermediate **III**. This step occurs first becomes evident from the experimental observation that in presence of base complete self-coupling of arylboronic acid to corresponding biaryl in 90% yield and no trace of arylation at indole was observed (Table **4A.1**, entry **20**). Then, in presence of strong π-nucleophile indole (**IV**), electrophilic palladation takes place at the C3 position of the indole ring (the most nucleophilic center on the indole nucleus) to form an intermediate species **V**, which undergoes 1,2-migration. The driving force for this C3→C2 migration is related to stabilization of the C–Pd bond

provided by the adjacent nitrogen atom at the C2 position (**VI**) [42,43]. Such metal migration around the aromatic nucleus and higher stability of organometallic intermediates when the metal is attached to an electron-deficient carbon centre has been well-identified and accepted in the literature [42]. The subsequent deprotonation forms intermediate **VII** and reductive elimination of the later species forms 2-arylated indole (**VIII**) with the regeneration of Pd(0) to complete the catalytic cycle. The mechanism makes the fact clear why electron-rich indoles facilitate the arylation process better than electron-poor indoles as the latter is less prone to electrophilic attack.

4A.3 Summary

In this section, a catalytic methodology has been demonstrated for the direct C2-arylation of indoles with arylboronic acids using a relatively cheap and readily available form of palladium. AgTFA has been used as an oxidant in the process. The experimental observation shows true heterogeneity of the active catalyst species. The protocol offers substantial benefits as achieving high C2 selectivity without the use of any ligands or directing groups and reusability of the catalyst with the retention of catalytic efficiency.

4A.4 Experimental Section

4A.4.1 General Information

All reactions were carried out in Tarsons spinot digital magnetic stirrers under standard conditions. Analytical thin layer chromatography (TLC) was carried out on Merck silica gel $60F_{254}$ plates using short wave (254 nm) and long wave (365 nm) UV light. Column chromatography purifications were performed over silica gel (100-200 mesh) and ethyl acetate/hexane as eluent. ^{1}H NMR and ^{13}C NMR spectra were recorded on a JEOL JNM ECS NMR spectrometer (400 MHz and 100 MHz respectively) using $CDCl_3$ as solvent and TMS as internal standard. The raw data of NMR were processed by MestReNova software. Chemical shifts (δ) are reported in ppm relative to the central peak of the solvent ($CDCl_3$: ^{1}H NMR, δ = 7.25 ppm and sometimes δ = 1.56 ($CDCl_3$-water); and ^{13}C NMR, δ = 77.0 ppm) and TMS (0 ppm). Multiplicities are indicated as: s (singlet), d (doublet), t (triplet), q (quartet), m (multiplet) and dd (doublet of doublet). Coupling constants (J values) are given in hertz (Hz). XPS

measurements were carried out using a Thermo-Scientific ESCALAB Xi+ spectrometer having a monochromatic Al Kα X-ray source (1486.6 eV) and a spherical energy analyzer that operates in the CAE (constant analyzer energy) mode. The CAE for the survey spectrum is 200 eV and that for high-resolution spectra is 50 eV. ICP-AES analysis was performed on an ACROS ICP spectrometer. Melting points were determined with a Buchi-535 apparatus and were not corrected. All chemicals used were purchased commercially from either Sigma Aldrich, Merck or Alfa Aesar and used without further purification. Solvents used for extraction and chromatographic separations were distilled prior to use.

4A.4.2 Synthesis of *N*-Substituted Indoles

N-substituted indoles were prepared following the procedure discussed in Chapter **3**.

4A.4.3 General Procedure for C2-Arylation of Indoles with Arylboronic Acids

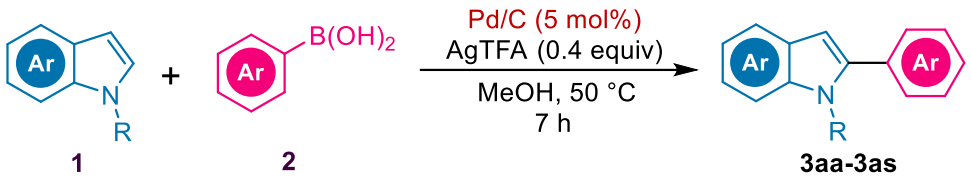

A round-bottom flask was charged with indole **1** (1 mmol) and arylboronic acid **2** (1.2 mmol) in presence of 10% Pd/C (5 mol%, 0.0053 g) and AgTFA (0.4 mmol, 0.088 g) in MeOH (1 mL) at 50 °C for 7 h in air. Progress and completion of reaction was confirmed by TLC in short wave (254 nm) and long wave (365 nm) UV light. The reaction mixture was evaporated to remove the solvent MeOH, followed by extraction with ethyl acetate and water. The organic layer was dried over anhydrous Na_2SO_4 and concentrated under reduced pressure. The residue was purified by column chromatography to give the desired products **3aa-3as**.

For ***reusability experiments***, the heterogeneous catalyst particles were recovered from the reaction media by centrifugation (600 rpm) and subsequently washed with water and ethyl acetate. The resultant catalyst particles were dried under vacuum and subjected to subsequent reaction runs.

4A.5 Characterization Data of the Products

1-Methyl-2-phenyl-1H-indole

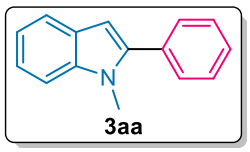

Obtained as white solid, 178 mg, 86% yield; mp 98-100 °C; ^{1}H NMR (400 MHz, $CDCl_3$), δ (ppm): 7.64 (d, J = 8.0 Hz, 1H), 7.52-7.44 (m, 4H), 7.41-7.35 (m, 2H), 7.25 (t, J = 8.2 Hz, 1H), 7.14 (t, J = 7.4 Hz, 1H), 6.56 (s, 1H), 3.74 (s, 3H); ^{13}C{^{1}H} NMR (100 MHz, $CDCl_3$), δ (ppm): 141.5, 138.3, 132.8, 129.3, 128.5, 127.9, 127.8, 121.6, 120.5, 119.8, 109.6, 101.6, 31.1.

2-(4-Methoxyphenyl)-1-methyl-1H-indole

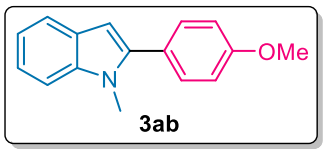

Obtained as white solid, 206 mg, 87% yield; mp 118-120 °C; ^{1}H NMR (400 MHz, $CDCl_3$), δ (ppm): 7.62 (d, J = 7.8 Hz, 1H), 7.48-7.41 (m, 2H), 7.34 (d, J = 8.2 Hz, 1H), 7.23 (t, J = 7.1 Hz, 1H), 7.13 (t, J = 7.8 Hz, 1H), 7.00-6.94 (m, 2H), 6.50 (s, 1H), 3.86 (s, 3H), 3.71 (s, 3H); ^{13}C{^{1}H} NMR (100 MHz, $CDCl_3$), δ (ppm): 159.4, 141.4, 138.1, 130.6, 127.9, 125.2, 121.3, 120.2, 119.7, 113.8, 109.5, 100.9, 55.3, 31.0.

2-(4-Chlorophenyl)-1-methyl-1H-indole

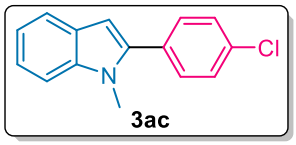

Obtained as colorless liquid, 196 mg, 81% yield; ^{1}H NMR (400 MHz, $CDCl_3$), δ (ppm): 7.64 (d, J = 6.0 Hz, 1H), 7.44 (m, 4H), 7.36 (d, J = 8.2 Hz, 1H), 7.28-7.24 (m, 1H), 7.15 (t, J = 7.2 Hz, 1H), 6.55 (s, 1H), 3.73 (s, 3H); ^{13}C{^{1}H} NMR (100 MHz, $CDCl_3$), δ (ppm): 140.2, 138.4, 134.0, 131.3, 130.5, 128.7, 127.8, 121.9, 120.5, 120.0, 109.6, 102.0, 31.2.

2-(4-Fluorophenyl)-1-methyl-1H-indole

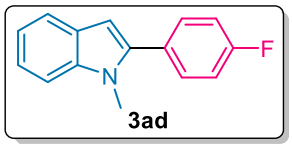

Obtained as pale yellow solid, 174 mg, 77% yield; mp 118-120 °C; ^{1}H NMR (400 MHz, $CDCl_3$), δ (ppm): 7.63 (d, J = 7.8 Hz, 1H), 7.48-7.44 (m, 2H), 7.35 (d, J = 7.7 Hz, 1H), 7.27-7.23 (m, 1H), 7.17-7.13 (m, 3H), 6.52 (s, 1H), 3.71 (s, 3H); ^{13}C{^{1}H} NMR (100 MHz, $CDCl_3$), δ (ppm): 162.6 (d, J = 248.3 Hz), 140.4, 138.2, 131.1 (d, J = 8.6 Hz), 128.9, 127.8, 121.7, 120.5, 119.8, 115.5 (d, J = 22.1 Hz), 109.6, 101.6, 31.1.

1-Methyl-2-(m-tolyl)-1H-indole

Obtained as colorless liquid, 184 mg, 83% yield; ^{1}H NMR (400 MHz, $CDCl_3$), δ (ppm): 7.63 (d, J = 8.8 Hz, 1H), 7.37-7.29 (m, 4H), 7.26-7.20 (m, 2H), 7.14 (t, J = 7.9 Hz, 1H),

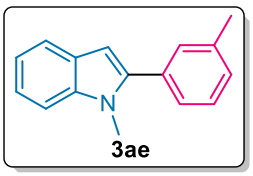

6.55 (s, 1H), 3.73 (s, 3H), 2.42 (s, 3H); $^{13}C\{^{1}H\}$ NMR (100 MHz, $CDCl_3$), δ (ppm): 141.7, 138.3, 138.2, 132.6, 130.1, 128.7, 128.3, 127.8, 126.4, 121.6, 120.4, 119.8, 109.6, 101.5, 31.1, 21.5.

1-Methyl-2-(3-nitrophenyl)-1H-indole

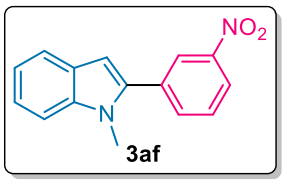

Obtained as yellow solid, 222 mg, 88% yield; mp 138-140 °C; ^{1}H NMR (400 MHz, $CDCl_3$), δ (ppm): 8.40 (s, 1H), 8.27 (dd, J = 8.2, 3.3 Hz, 1H), 7.86 (d, J = 7.7 Hz, 1H), 7.67 (t, J = 7.9 Hz, 2H), 7.41 (d, J = 8.3 Hz, 1H), 7.32 (t, J = 8.2 Hz, 1H), 7.19 (t, J = 7.4 Hz, 1H), 6.68 (s, 1H), 3.80 (s, 3H); $^{13}C\{^{1}H\}$ NMR (100 MHz, $CDCl_3$), δ (ppm): 148.4, 138.7, 138.6, 134.9, 134.5, 129.6, 127.7, 123.8, 122.6, 122.5, 120.9, 120.3, 109.8, 103.3, 31.3.

1-Methyl-2-(3-(trifluoromethyl)phenyl)-1H-indole

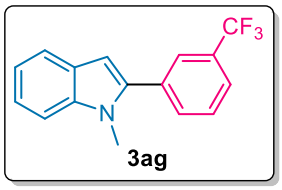

Obtained as yellow liquid, 201 mg, 73% yield; ^{1}H NMR (400 MHz, $CDCl_3$), δ (ppm): 7.78 (s, 1H), 7.70-7.64 (m, 3H), 7.59 (t, J = 7.7 Hz, 1H), 7.38 (d, J = 8.2 Hz, 1H), 7.28 (t, J = 8.2 Hz, 1H), 7.17 (t, J = 7.4 Hz, 1H), 6.62 (s, 1H), 3.75 (s, 1H); $^{13}C\{^{1}H\}$ NMR (100 MHz, $CDCl_3$), δ (ppm): 139.8, 138.6, 133.6, 132.4 (q, J = 32.0 Hz), 131.2, 130.9, 129.0, 127.8, 125.9 (q, J = 3.9 Hz), 124.4 (q, J = 270.6 Hz), 122.1, 120.7, 120.1, 109.7, 102.6, 31.2.

1-(4-(1-Methyl-1H-indol-2-yl)phenyl)ethan-1-one

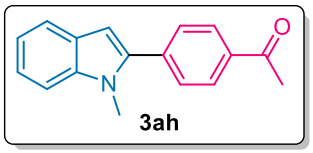

Obtained as yellow solid, 175 mg, 70% yield; mp 121-124 °C; ^{1}H NMR (400 MHz, $CDCl_3$), δ (ppm): 8.06 (d, J = 8.6 Hz, 2H), 7.66-7.61 (m, 3H), 7.38 (d, J = 8.3 Hz, 1H), 7.28 (t, J = 7.0 Hz, 1H), 7.16 (t, J = 7.3 Hz, 1H), 6.66 (s, 1H), 3.78 (s, 3H), 2.65 (s, 3H); $^{13}C\{^{1}H\}$ NMR (100 MHz, $CDCl_3$), δ (ppm): 197.6, 140.2, 138.8, 137.4, 136.0, 129.1, 128.6, 127.8, 122.4, 120.8, 120.1, 109.7, 102.9, 31.5, 26.6.

1-Methyl-2-(o-tolyl)-1H-indole

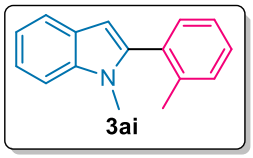

Obtained as white solid, 173 mg, 78% yield; mp 88-90 °C; ^{1}H NMR (400 MHz, $CDCl_3$), δ (ppm): 7.65 (d, J = 7.5 Hz, 1H), 7.38-7.25 (m, 6H), 7.16 (t, J = 7.4 Hz, 1H), 6.43 (s, 1H), 3.52 (s, 3H),

2.21 (s, 3H); $^{13}C\{^{1}H\}$ NMR (100 MHz, $CDCl_3$), δ (ppm): 141.7, 138.3, 138.2, 132.7, 130.1, 128.6, 128.3, 127.9, 126.4, 121.5, 120.4, 119.8, 109.6, 101.5, 31.2, 21.5.

2-(4-(tert-Butyl)phenyl)-1-methyl-1H-indole

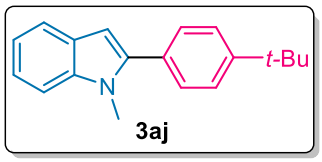

Obtained as white solid, 224 mg, 85% yield; mp 108-110 °C; ^{1}H NMR (400 MHz, $CDCl_3$), δ (ppm): 7.62 (d, J = 7.8 Hz, 1H), 7.46 (q, J = 8.6 Hz, 4H), 7.35 (d, J = 8.2 Hz, 1H), 7.23 (t, J = 7.0 Hz, 1H), 7.13 (t, J = 7.0 Hz, 1H), 6.54 (s, 1H), 3.74 (s, 3H), 1.37 (s, 9H); $^{13}C\{^{1}H\}$ NMR (100 MHz, $CDCl_3$), δ (ppm): 150.9, 141.6, 138.3, 129.9. 129.0, 128.0, 125.4, 121.4, 120.3, 119.7, 109.5, 101.3, 58.2, 34.7, 31.3.

5-Methoxy-1-methyl-2-phenyl-1H-indole

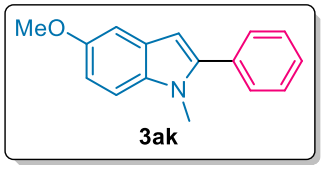

Obtained as white solid, 200 mg, 84% yield; mp 115-117 °C; ^{1}H NMR (400 MHz, $CDCl_3$), δ (ppm): 7.51-7.37 (m, 5H), 7.25 (d, J = 8.9 Hz, 1H), 7.10 (d, J = 2.4 Hz, 1H), 6.91 (dd, J = 8.9, 2.5 Hz, 1H), 6.49 (s, 1H), 3.86 (s, 3H), 3.71 (s, 3H); $^{13}C\{^{1}H\}$ NMR (100 MHz, $CDCl_3$), δ (ppm): 154.3, 142.2, 133.8, 132.9, 129.2, 128.5, 128.2, 127.8, 111.9, 110.3, 102.1, 101.2, 56.0, 31.2.

5-Methoxy-2-(4-methoxyphenyl)-1-methyl-1H-indole

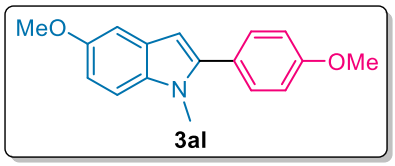

Obtained as white solid, 233 mg, 87% yield; mp 111-113 °C; ^{1}H NMR (400 MHz, $CDCl_3$), δ (ppm): 7.42 (d, J = 8.9 Hz, 2H), 7.25 (s, 1H), 7.09 (d, J = 2.5 Hz, 1H), 7.00 (d, J = 8.7 Hz, 2H), 6.89 (dd, J = 8.8, 2.5 Hz, 1H), 6.42 (s, 1H), 3.87 (s, 6H), 3.69 (s, 3H); $^{13}C\{^{1}H\}$ NMR (100 MHz, $CDCl_3$), δ (ppm): 159.4, 154.3, 142.0, 133.6, 130.5, 128.2, 125.3, 113.9, 111.5, 110.2, 102.0, 100.6, 55.9, 55.3, 31.1.

1,3-Dimethyl-2-phenyl-1H-indole

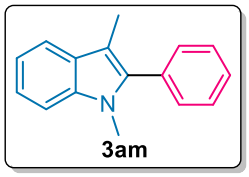

Obtained as colorless liquid, 182 mg, 82% yield; ^{1}H NMR (400 MHz, $CDCl_3$), δ (ppm): 7.60 (d, J = 7.8 Hz, 1H), 7.49 (t, J = 6.6 Hz, 2H), 7.41 (t, J = 6.8 Hz, 3H), 7.33 (d, J = 8.2 Hz, 1H), 7.25 (t, J = 7.6 Hz, 1H), 7.15 (t, J = 7.4 Hz, 1H), 3.61 (s, 3H), 2.28 (s, 3H); $^{13}C\{^{1}H\}$ NMR (100 MHz, $CDCl_3$), δ (ppm): 137.6, 137.2, 132.1, 130.6, 128.4, 128.3, 127.7, 121.7, 119.1, 118.8, 109.2, 108.6, 30.9, 9.1.

1,7-Dimethyl-2-phenyl-1H-indole

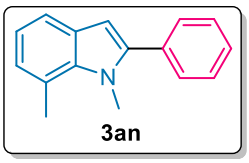

Obtained as white solid, 195 mg, 88% yield; mp 67-69 °C; ^{1}H NMR (400 MHz, $CDCl_3$), δ (ppm): 7.50-7.43 (m, 5H), 7.41-7.37 (m, 1H), 7.00 (t, J = 7.4 Hz, 1H), 6.94 (d, J = 6.8 Hz, 1H), 6.51 (s, 1H), 3.92 (s, 3H), 2.81 (s, 3H); ^{13}C{^{1}H} NMR (100 MHz, $CDCl_3$), δ (ppm): 142.7, 137.6, 133.0, 129.6, 128.8, 128.3, 124.6, 121.4, 120.0, 118.7, 102.4, 99.8, 34.4, 20.1.

1-Benzyl-2-phenyl-1H-indole

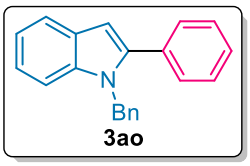

Obtained as colorless liquid, 255 mg, 90% yield; ^{1}H NMR (400 MHz, $CDCl_3$), δ (ppm): 7.68-7.66 (m, 1H), 7.45-7.42 (m, 2H), 7.40-7.36 (m, 3H), 7.29-7.22 (m, 3H), 7.17-7.13 (m, 3H), 7.03 (d, J = 6.6 Hz, 2H), 6.65 (s, 1H), 5.36 (s, 2H); ^{13}C{^{1}H} NMR (100 MHz, $CDCl_3$), δ (ppm): 141.8, 138.2, 137.9, 132.7, 129.2, 128.7, 128.5, 128.3, 128.0, 127.1, 125.9, 121.9, 120.5, 120.1, 110.5, 102.3, 47.7.

5-Chloro-1-methyl-2-phenyl-1H-indole

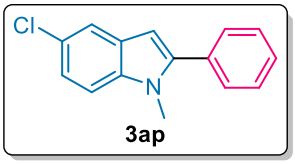

Obtained as white solid, 164 mg, 68% yield; mp 87-88 °C; ^{1}H NMR (400 MHz, $CDCl_3$), δ (ppm): 7.59 (d, J = 2.0 Hz, 1H), 7.49-7.41 (m, 5H), 7.26 (t, J = 8.7 Hz, 1H), 7.18 (dd, J = 8.7, 2.0 Hz, 1H), 6.49 (s, 1H), 3.72 (s, 3H); ^{13}C{^{1}H} NMR (100 MHz, $CDCl_3$), δ (ppm): 142.8, 136.7, 132.3, 129.3, 128.8, 128.6, 128.2, 125.4, 121.8, 119.8, 110.6, 101.1, 31.2.

5-Bromo-1-methyl-2-phenyl-1H-indole

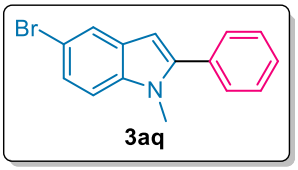

Obtained as white solid, 186 mg, 65% yield; mp 108-110 °C; ^{1}H NMR (400 MHz, $CDCl_3$), δ (ppm): 7.75 (d, J = 1.9 Hz, 1H), 7.50-7.40 (m, 5H), 7.31 (dd, J = 8.7, 1.9 Hz, 1H), 7.22 (t, J = 8.7 Hz, 1H), 6.49 (s, 1H), 3.71 (s, 3H); ^{13}C{^{1}H} NMR (100 MHz, $CDCl_3$), δ (ppm): 142.7, 137.0, 132.2, 129.5, 129.3, 128.5, 128.2, 124.2, 122.8, 113.0, 110.9, 100.9, 31.2.

1-Methyl-2-phenyl-1H-pyrrolo[2,3-b]pyridine

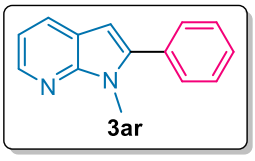

Obtained as colorless liquid, 148 mg, 71% yield; ^{1}H NMR (400 MHz, $CDCl_3$), δ (ppm): 8.35 (dd, J = 4.7, 1.5 Hz, 1H), 7.91 (dd, J = 7.8, 1.6 Hz, 1H), 7.58–7.42 (m, 5H), 7.10 (dd, J = 7.8, 4.7 Hz, 1H),

6.52 (s, 1H), 3.89 (s, 3H); $^{13}C\{^{1}H\}$ NMR (100 MHz, $CDCl_3$), δ (ppm): 149.2, 142.6, 141.9, 132.3, 129.1, 128.6, 128.3, 128.2, 120.7, 116.1, 99.4, 29.9.

1-Methyl-2,5-diphenyl-1H-pyrrole

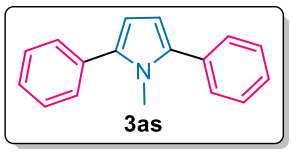

Obtained as white solid, 175 mg, 75% yield; mp 198-200 °C; ^{1}H NMR (400 MHz, $CDCl_3$), δ (ppm): 7.48 (dd, J = 8.3, 1.4 Hz, 4H), 7.44-7.40 (m, 4H), 7.33-7.29 (m, 2H), 6.32 (s, 2H), 3.61 (s, 3H); $^{13}C\{^{1}H\}$ NMR (100 MHz, $CDCl_3$), δ (ppm): 136.9, 133.5, 128.7, 128.4, 126.6, 108.7, 34.4.

4A.6 Representative ^{1}H and $^{13}C\{^{1}H\}$ NMR spectra

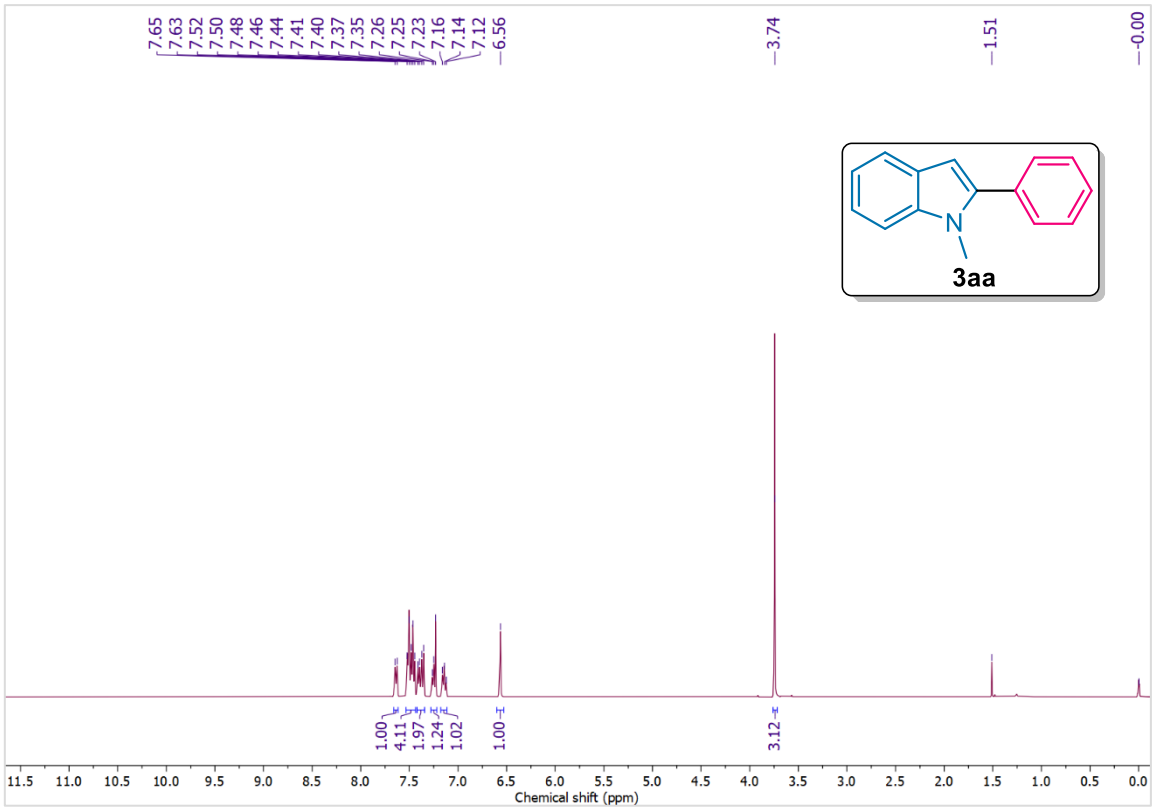

Figure 4A.3 ^{1}H NMR (400 MHz) spectrum of **3aa** in $CDCl_3$

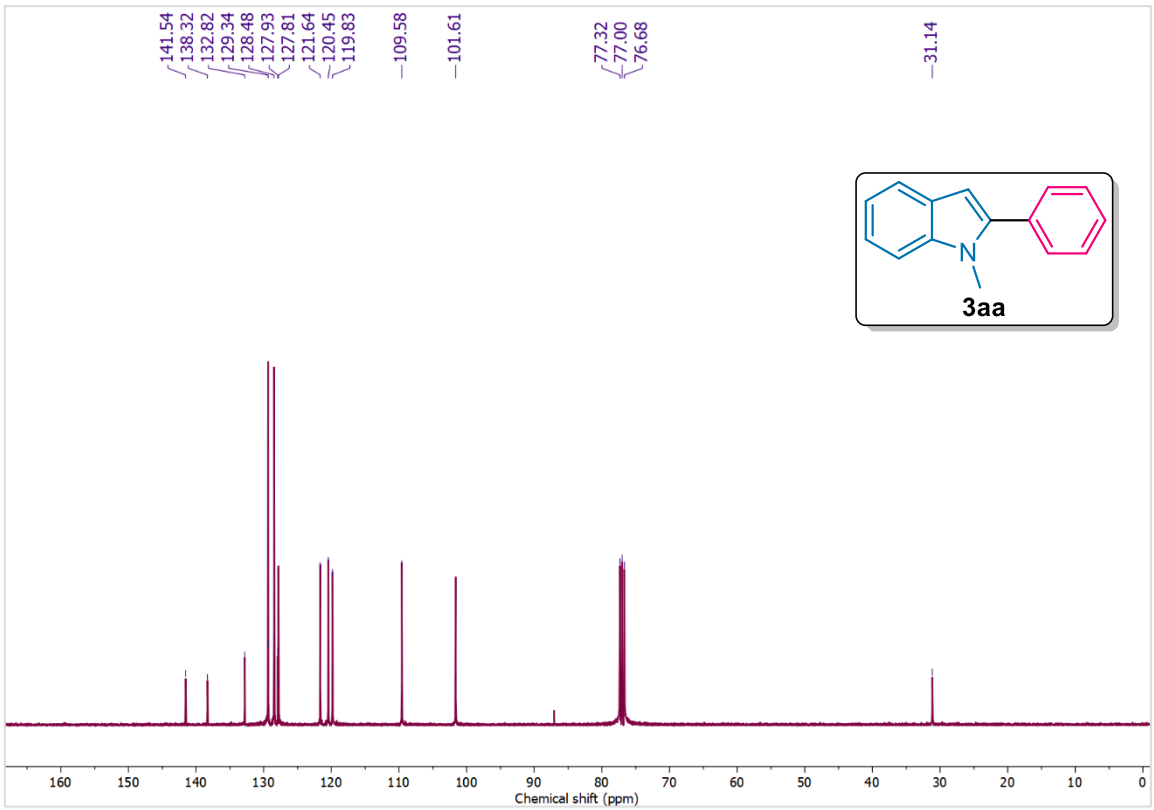

Figure 4A.4 $^{13}C\{^{1}H\}$ NMR (100 MHz) spectrum of **3aa** in $CDCl_3$

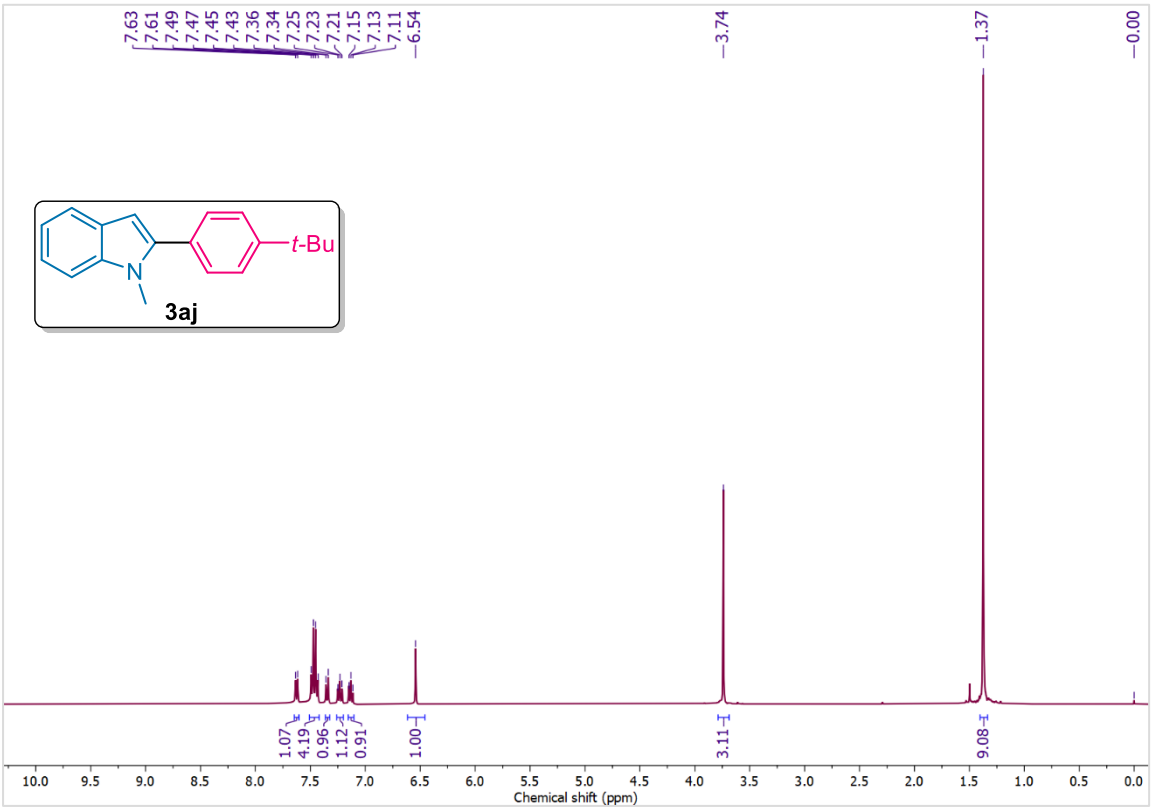

Figure 4A.5 ^{1}H NMR (400 MHz) spectrum of **3aj** in $CDCl_3$

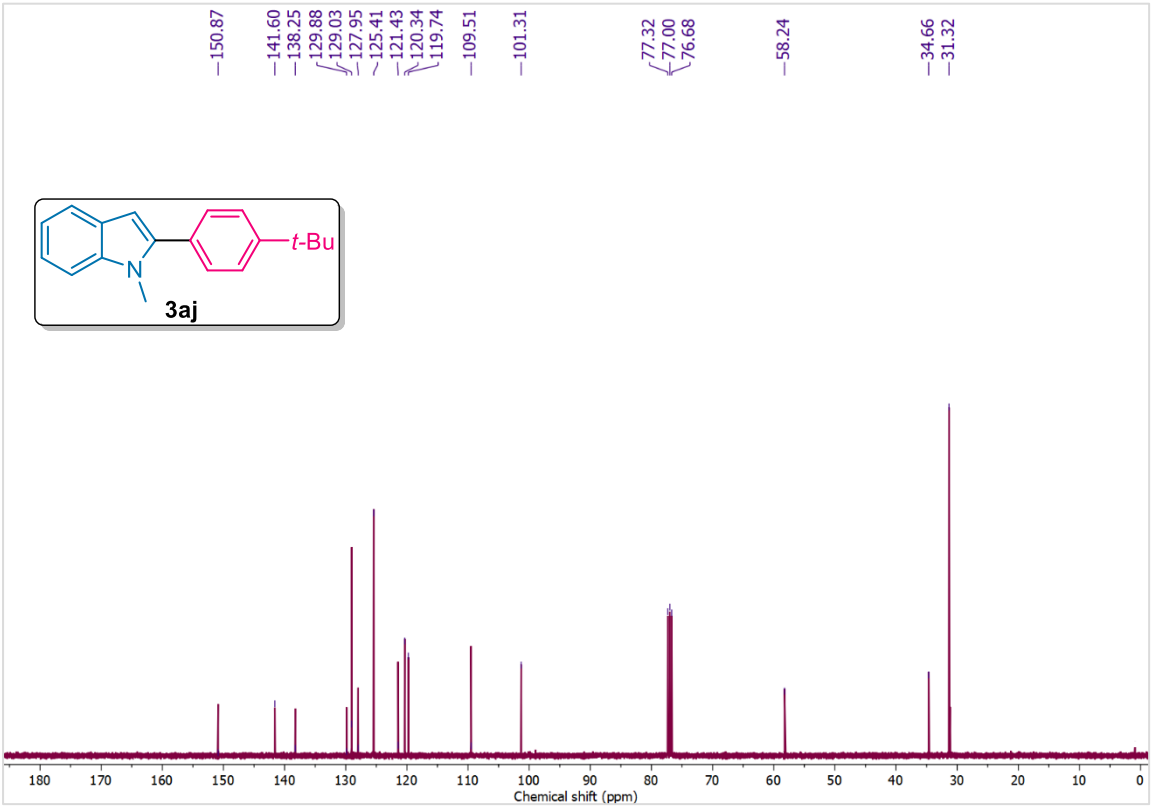

Figure 4A.6 $^{13}C\{^{1}H\}$ NMR (100 MHz) spectrum of **3aj** in $CDCl_3$

Section B

Pd(0)-Embedded-Lignocellulosic Nanomaterials: A Bio-Tailored Reusable Catalyst for Selective C2-Arylation of Free N–H Indoles

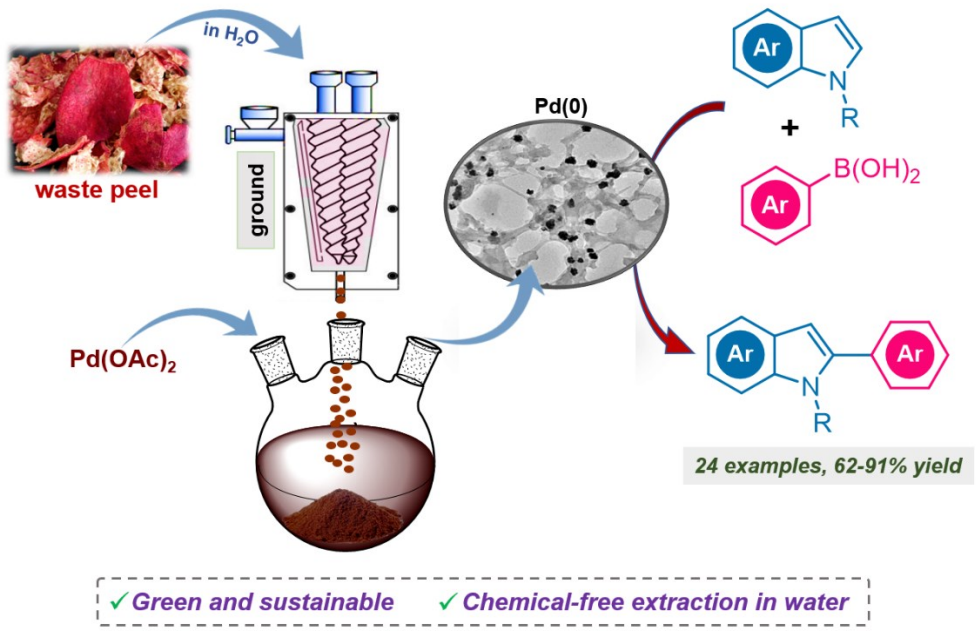

4B.1 Introduction

Chapter **4** Section **A** explored the catalytic viability of commercial heterogeneous Pd supported on carbon (Pd/C) towards the C2-functionalization of indoles. Although several types of nano-porous materials have been used for incorporating metal nanoparticles (NPs), however last decade has witnessed innumerable potential in biomass and biomass-derived materials as promising candidates [44,45]. Being the nature's most abundant bio-renewable and sustainable source of organic carbon, lignocellulosic biomass has gained enormous importance due to their wide availability, easy accessibility, high adsorption ability and eco-friendly characters [46].

Structural framework of lignocellulosic biomass is mainly composed of three bio-polymers; cellulose, hemicellulose, and lignin [47], organized in complex non-uniform 3D structures varying to different degrees and relative composition depending on the bio-precursor [48]. Its unique structural features and versatility hold enormous prospective for employing it as a suitable support material for metal nanoparticles. Much of the current research is prevalently focused on lignocellulosic fractionation into its three major components [49,50]. Achieving this goal can be quite tricky as nature has developed this bio-polymer to resist degradation. This inherent structural robustness has accounted from the crystallinity of cellulose, hydrophobicity of lignin, and encapsulation of cellulose by the lignin-hemicellulose environment [47]. Thus, for modifying the natural binding characteristics of supramolecular lignocellulose matrix, along with their physical and chemical properties; various pre- and post-treatment methods need to be processed [51,52]. Although lignocellulosic materials are abundant and low-priced, the critical challenge is scaling up of the current laboratory-scale synthetic methods, as the pre-treatments of biomass are energy-intensive, consuming large quantity of toxic chemicals, harsh conditions, and involving multiple steps, which questions their sustainability [52]. The existing issue, therefore, is to develop an efficient support material in a manner that is environmentally sustainable and can be easily scaled up to industrial level.

Punica granatum commonly known as pomegranate fruit has shown an explosion of production as a super-fruit due to rising awareness on its nutritional and therapeutic

values [53,54]. The large organic proportions of non-edible part of the fruit, comprising peel and internal membranes, serves as a vital lignocellulosic feedstock.

Table 4B.1 Pd-based heterogeneous catalysts explored for C2-arylation of indoles

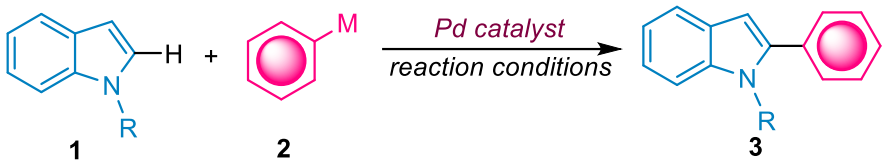

Entry [ref.]	Catalyst; Reaction parameters [M/reagents/solvent/T]	Catalyst preparation approach
1 [34]	NHC-Pd@MNPs; [I/NaOAc/DMSO/120 °C]	Multi-step chemical synthetic approach for formulating *N*-heterocyclic carbene supported magnetic Pd NPs; process temperature up to 110 °C.
2 [29]	Pd@UiO-66-BTeC; [$ArI^+ BF_4^-$/GVL/80 °C]	MOF prepared using mixed linker-ligating group strategy *via* chemical approach at 100-190 °C.
3 [30]	Pd/11.5 ODDMA-MP; [$ArI^+ OTf^-$/H_2O/60 °C]	Mesoporous resin-polymeric support synthesized *via* surfactant-templating method; step-wise thermo-polymerization performed at 100-275 °C.
4 [31]	Pd/MIL-101; [$B(OH)_2$/O_2/DCM-AcOH/ 60 °C]	Incorporation of Pd NPs in MIL-101 *via* solution infiltration and H_2 treatment at 200 °C.
5	10% Pd/C; [$B(OH)_2$/AgTFA/MeOH/ 50 °C]	Commercially available; but commercial preparations involve chemical approach. (Section **A**)
6	Pd NPs@LCpp; [$B(OH)_2$/AgTFA/ MeOH-H_2O/50 °C]	Lignocellulose support derived from waste pomegranate peels *via* greener, approach at rt, with Pd(0) generation and loading in one-step. (This Section)

In a recent study conducted by Nejib Hasnaoui and co-workers on the composition of pomegranate peel fibers obtained from 12 different cultivars, it was found that all the 12 varieties contained a relatively higher lignin content (20.59-41.86 g) compared to cellulose (16.53-22.71 g) of 100 g of extracted peel fibers [55]. Thus, the current

search for an appropriate supported Pd nanomaterials, provoked the study in this section to utilize this resource-efficient raw lignocellulosic waste derived from pomegranate peels (LCpp) as an eco-friendly support matrix for Pd nanoparticles (Pd NPs@LCpp), without disturbing its natural bio-structure.

As documented in Chapter **4** Section **A**, most of the methods reported in the literature for direct C2-arylation of indoles using heterogeneous Pd catalysts [28-34], involve chemical-approach for catalyst design demanding toxic chemical usage and high temperature preparations (Table **4B.1**). Application of Pd bio-nanomaterials from non-food lignocellulosic feedstocks is new to this field and shows immense potential and scope. With the intention of extending further on the study of C2-arylation of indoles, this section proposes to investigate the activity of Pd NPs@LCpp towards the arylation process without resorting to any directing group strategy.

4B.2 Results and Discussion

4B.2.1 Preparation of Lignocellulose-Supported Pd Nanomaterials

Facile synthesis of Pd NPs@LCpp was achieved in which Pd NPs are supported on lignocellulose support (LCpp) derived from the waste biomass feedstock of pomegranate peels. During the preparation, neither biomass pre-treatments nor chemical reducing agents were used in the process. The inherent porosity and presence of high density hydrophilic functional groups, such as carbonyl, hydroxyl and carboxyl groups make lignocellulose material a prominent capping agent for anchoring and stabilization of noble nano materials on the bio-support [56].

4B.2.2 Characterization of Pd NPs@LCpp

The formation of Pd NPs@LCpp was confirmed by analytical techniques namely, scanning electron microscopy (SEM), transmission electron microscopy (TEM), energy dispersive X-Ray (EDX), powder X-ray diffraction (PXRD), Fourier transform infrared (FT-IR) spectroscopy, inductively coupled plasma-optical emission spectrometry (ICP-OES), X-ray photoelectron spectroscopy (XPS), and Brunauer-Emmett-Teller (BET) surface area analyses.

The surface morphology of the microstructures was imaged by SEM. The micrograph of pure LCpp (Figure **4B.1a-b**) showed irregular appearance with un-separated fiber

bundles of cellulose, hemicellulose, and lignin. The bundles are nearly 100-140 µm long and 20-30 µm thick. The presence of small pores on the rough exterior of biomass facilitates the binding of Pd NPs onto it. The image of Pd NPs@LCpp (Figure **4B.1c-e**) showed highly loaded and well-dispersed Pd NPs distributed evenly over the bio-surface. Consistently, the EDX elemental mapping images (Figure **4B.1f-h**) showed the uniform dispersal and overlapping of C, Pd, and O throughout the sample, thus confirming the homogeneous distribution of Pd NPs on LCpp.

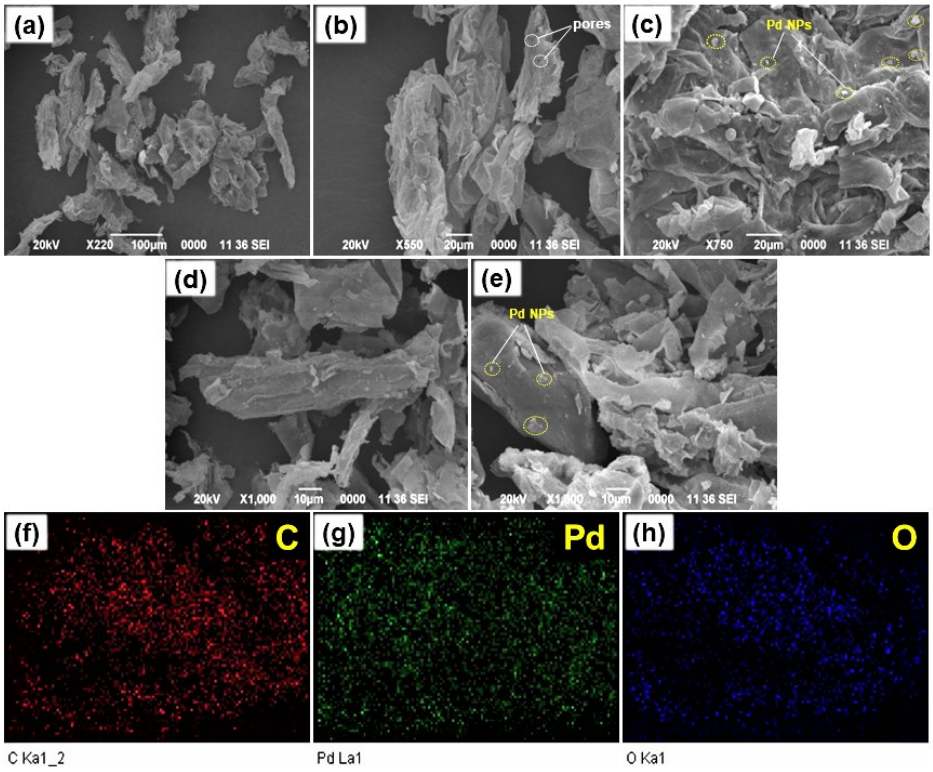

Figure 4B.1 SEM micrographs of (a-b) LCpp, (c-e) Pd NPs@LCpp, and corresponding (f-h) EDX elemental mapping images

The low-resolution TEM of Pd NPs@LCpp (Figure **4B.2a-c**) showed the prominent existence of Pd NPs entangled in the lignocellulose bio-network which stabilizes their dispersion. The particle size distribution curve (Figure **4B.2d**) shows that the Pd NPs embedded in the biomass support are homogeneous in size (~43 nm). High-resolution TEM (HRTEM) images of the Pd NPs (Figure **4B.2e**) shows the presence of lattice fringes with spacing 0.112 nm, 0.137 nm, and 0.225 nm, which are consistent with (222), (220), and (111) crystallographic planes of Pd respectively. The crystalline structure of Pd NPs was further characterized by the selected area electron diffraction (SAED). The diffraction ring patterns with intermittent bright

dots (Figure **4B.2f**) are correspondingly assigned to (111), (200), (220), (311), and (222) crystalline lattice plane of fcc Pd(0) in accordance with JCPDS card no. 87-0641. These results reveal the efficient interaction, stabilization, and dispersal of Pd NPs by LCpp, thus defining the platform for lignocellulosic nanomaterials.

Furthermore, elemental composition of Pd NPs@LCpp was assessed by EDX analysis, which reveals the presence of Pd (2.18%) in the nanomaterial with a trace of some other elements. The existence of organic biomass backbone is confirmed by the intense peaks for C and O element which holds 67% and 30% atomic content of the total sample respectively (Figure **4B.2g**). Moreover, ICP-OES analysis revealed that 1 g of solid Pd NPs@LCpp contains 13 mg of Pd.

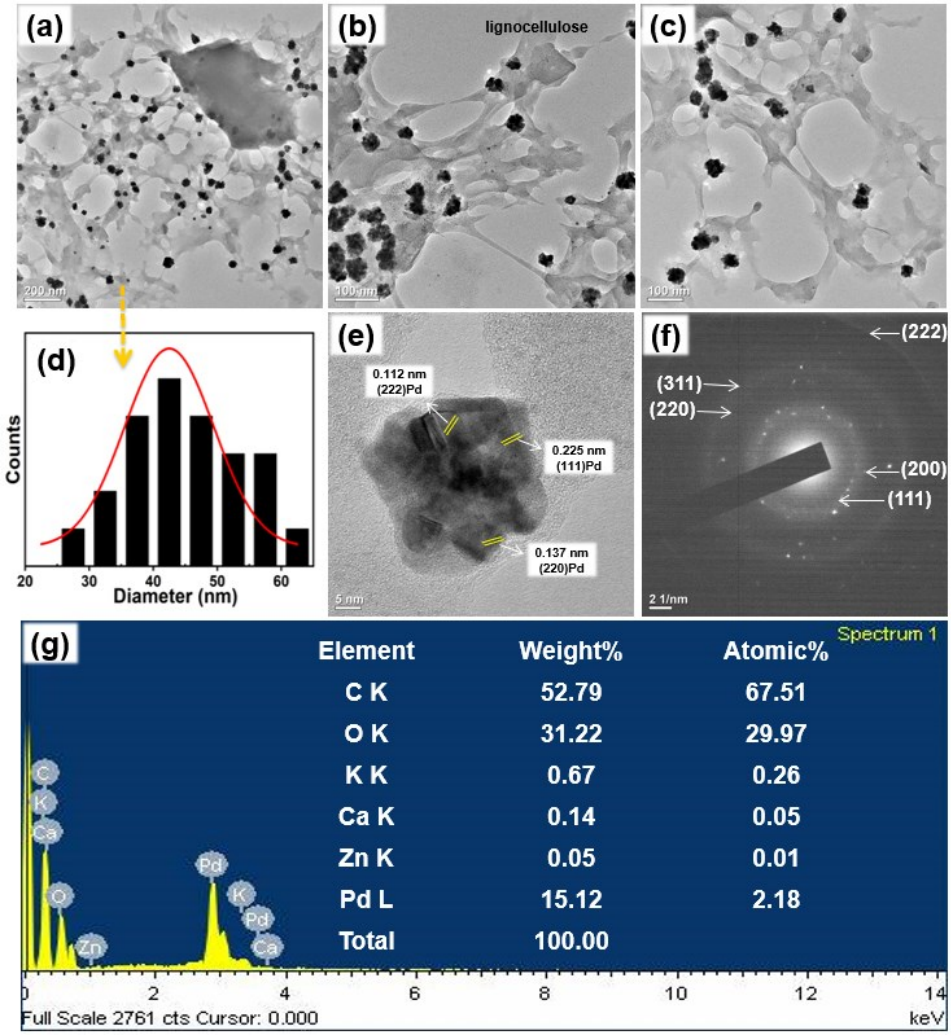

Figure 4B.2 (a-c) TEM images, (d) particle size distribution histogram, (e) HRTEM image, (f) SAED pattern, and (g) EDX image, of Pd NPs@LCpp

The surface elemental composition and the oxidation states of the constituent elements of Pd NPs@LCpp were determined by XPS analysis. The survey scans XPS spectrum of Pd NPs@LCpp suggest the existence of Pd, C, and O elements (Figure **4B.3a**). The high-resolution XPS spectrum for all these respective elements were recorded and deconvoluted as shown in Figure **4B.3b-d.** The high-resolution XPS spectrum of Pd 3d suggests the presence of both Pd(0) and Pd(II) in Pd NPs@LCpp (Figure **4B.3b**). The characteristic peaks at 333.9 eV and 339.3 eV were observed, which are ascribed to the spin-orbit splitting of Pd $3d_{5/2}$ and Pd $3d_{3/2}$ belonging to Pd(0), respectively and similarly for Pd(II) obtained at 336.1 eV and 341.3 eV, respectively [38]. The high-resolution C 1s spectrum was fitted with three different peaks at 284.6 eV, 286.3 eV, and 288.5 eV, corresponding to C–C/C=C, C–O, and C=O species respectively (Figure **4B.3c**). Moreover, high-resolution O 1s fitted with two binding energy peaks at 531 eV and 532.3 eV (assigned as O1 and O2) are ascribed to the lattice oxygen of oxidized PdO and chemisorbed oxygen functional groups of lignocellulose, respectively (**Figure 4B.3d**) [57].

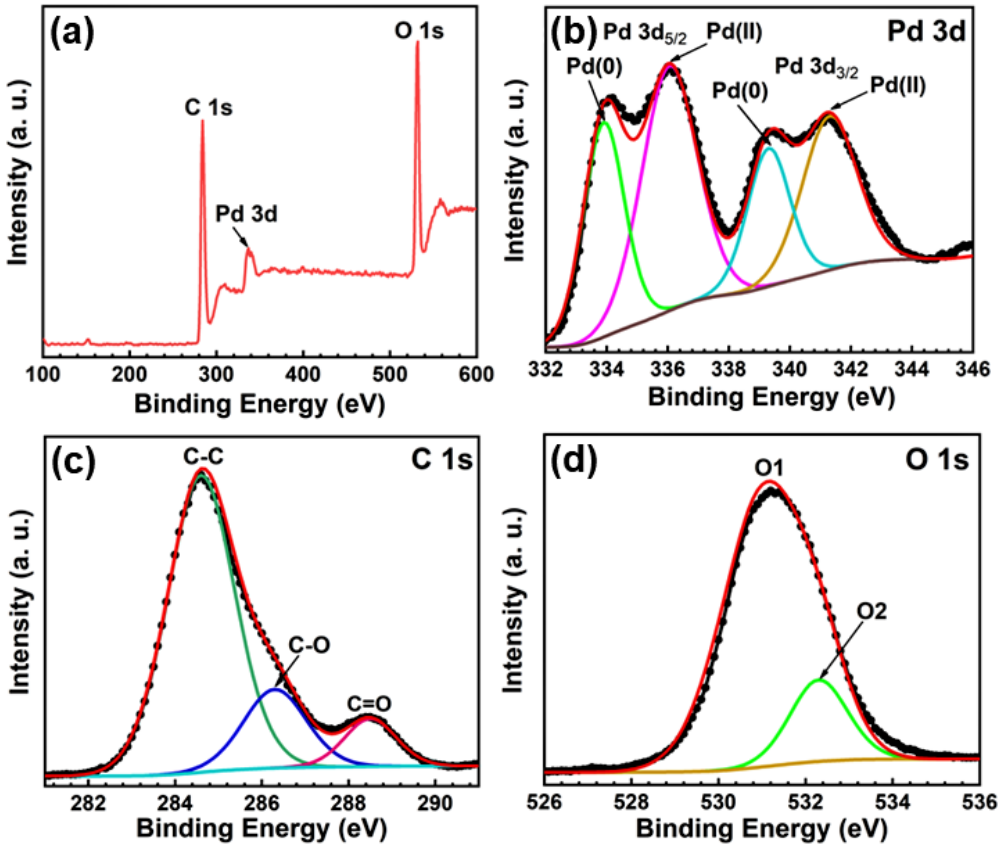

Figure 4B.3 (a) Survey scans XPS spectrum of Pd NPs@LCpp, and corresponding high-resolution XPS spectra of (b) Pd 3d, (c) C 1s, and (d) O 1s

The powder XRD patterns were analyzed to study the crystal phase information of lignocellulose-materials before and after metal fabrication (Figure **4B.4a**). The diffractograms of LCpp showed a broad peak under the curve which confirms the amorphous structural characteristic of biomass material. The diffraction peak at 2θ value of 21.98° signifies the (002) plane of organic carbon backbone in lignocellulose [58]. In comparison to LCpp, metal loaded Pd NPs@LCpp showed three intensive peaks (2θ) at 40.06°, 46.45°, 67.93°, which are respectively corresponded to (111), (200), (220), planes of Pd. These characteristic sharp peaks are consistent with the standard crystalline structure of Pd (JCPDS card no.- 87-0641). Thus, the incorporation of Pd NPs into bio-matrix causes a substantial change in crystallinity of the material.

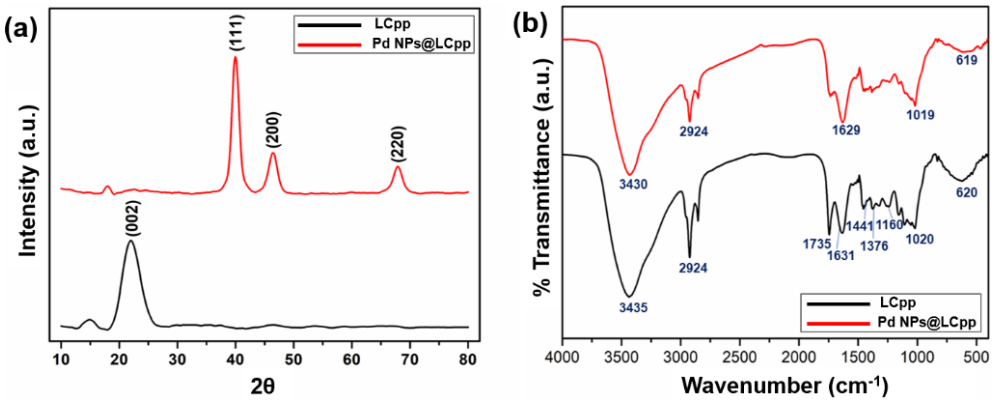

Figure 4B.4 (a) Powder XRD patterns, (b) FT-IR spectra, of LCpp and Pd NPs@LCpp

FT-IR spectra were recorded for LCpp before and after Pd metal loading (Figure **4B.4b**). The abundance of peaks for both the samples demonstrated the structural complexity in the bio-polymeric structures. In both the samples, a broad and intense peak centred around 3435 cm^{-1} is attributed to the O–H groups present in cellulose, hemicellulose, and lignin of the biomass. In addition, several peaks centred around 2924, 1735, 1631, 1441 and 1020 cm^{-1}, are assigned to the various stretching and bending vibrational modes of C–H, C=O, O–H, C–O in lignocellulose [46]. Presence of high-density oxygen-rich functional groups impart hydrophilic character to the bio-nanomaterials, resulting in better coordination and stabilization of NPs in the support. The similarity between the spectra suggests no significant change in the functionalities of biomass occurred on Pd loading. However, a slight shift in frequency of the bands correlates the interaction of functional groups to Pd NPs on the support.

The surface area and pore characteristics of lignocellulose materials were studied by BET N_2 adsorption-desorption isotherms at 77 K (Figure **4B.5**). The sorption curves resembling the classical type IV isotherm is obtained for both the samples. Appearance of H3 hysteresis loops in the relative pressure (P/P_0) range 0.4-0.9 represents the mesoporous nature of the materials [59]. The standard multi-point BET reveals the specific surface area of 52.247 m^2/g in LCpp (Figure **4B.5a**), which reduce significantly to 14.272 m^2/g in Pd NPs@LCpp (Figure **4B.5b**). This reveals the high adsorption efficiency of the bio-nanomaterial, resulting in a strong adsorbate (Pd NPs)-adsorbent (LCpp) interaction. Furthermore, immobilization of Pd NPs on the mesoporous structure of support was confirmed by BJH pore size distribution (inset Figure **4B.5a-b**), which reveals pore diameter of 2.863 nm in LCpp reduced to 2.440 nm in Pd NPs@LCpp.

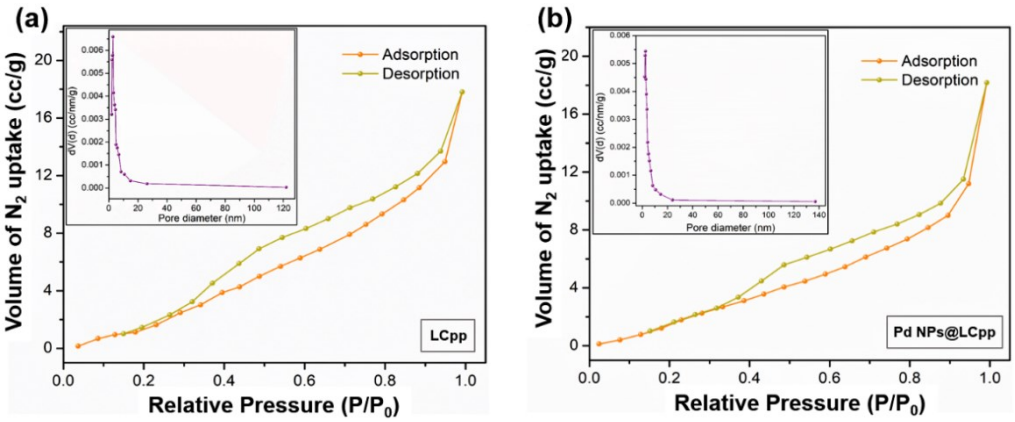

Figure 4B.5 N_2 adsorption/desorption isotherms of (a) LCpp, (b) Pd NPs@LCpp, and inset in (a, b) shows the BJH pore size distribution curves

4B.2.3 Optimization of Reaction Conditions

The catalytic effectiveness of the as-prepared Pd NPs@LCpp was evaluated in C2-arylation of indoles with arylboronic acids in the absence of any ligands or directing groups. The reaction is optimized using 1-methylindole (**1a**) and phenylboronic acid (**2a**) as the model arylating agents, as outlined in Table **4B.2**. Initially, a reaction was carried out using 15 wt% of the catalyst without using any oxidant. However, no product formation could be detected (Table **4B.2**, entry **1**). So, a variety of copper and silver salts have been tested in the catalytic system (Table **4B.2**, entries **2-6**). AgTFA was found to be most effective as oxidant for the present system resulting up to 85% of the C2-arylated product **3ba** in 7 h (Table **4B.2**, entry **2**).

Table 4B.2 Screening of reaction conditions for C2-arylation of indoles[a]

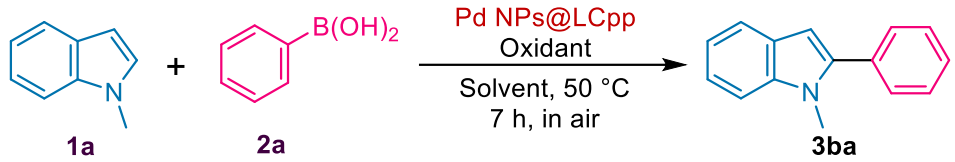

Entry	Catalyst (wt%)	Oxidant (mmol)	Solvent	Yield (%)[b] of **3ba**
1	15	-	MeOH	nr
2	15	AgTFA (0.8)	MeOH	85
3	15	AgOAc (0.8)	MeOH	37
4	15	$Cu(OAc)_2 \cdot H_2O$ (0.8)	MeOH	0
5	15	$Cu(OTf)_2$ (0.8)	MeOH	27
6	15	Ag_2O (0.8)	MeOH	0
7	15	AgTFA (0.5)	MeOH	85
8	15	AgTFA (0.4)	MeOH	81
9	15	AgTFA (0.2)	MeOH	68
10	10	AgTFA (0.5)	MeOH	86
11	8	AgTFA (0.5)	MeOH	83
12	5	AgTFA (0.5)	MeOH	76
13[c]	10	AgTFA (0.5)	MeOH	70
14[d]	10	AgTFA (0.5)	MeOH	58
15	10	AgTFA (0.5)	EtOH	76
16	10	AgTFA (0.5)	PEG-300	58
17	10	AgTFA (0.5)	H_2O	40
18	10	AgTFA (0.5)	MeOH-H_2O (2:1)	70
19[e]	10	AgTFA (0.5)	MeOH-H_2O (5:1)	91
20[f]	$Pd(OAc)_2$	AgTFA (0.5)	MeOH-H_2O (5:1)	82

[a]Reaction conditions: **1a** (1 mmol), **2a** (1.2 mmol), catalyst (Pd NPs@LCpp), oxidant (mmol), solvent (2 mL), T (50 °C), time (7 h), in air; [b]isolated yield; [c]T (40 °C); [d]N_2 atmosphere; [e]time (5 h); [f]$Pd(OAc)_2$ (1 mol%), time (8 h); nr (no reaction).

Now, to determine the optimum amount of AgTFA needed for this transformation, reactions were conducted by sequentially lowering its amount from 0.8 equiv to 0.5 equiv and 0.4 equiv of AgTFA (Table **4B.2**, entries **7**-**8**). It was observed that the reaction could maintain its effectiveness even with the reduced amounts of oxidant producing 80-85% yield of the C2-arylated product. Further lowering of AgTFA to 0.2 equiv (20 mol%) could also furnish 68% of the desired product (Table **4B.2**, entry **9**). The results exhibited an interesting fact that a very small amount of Ag oxidant is sufficient to perform the desired transformation. At this stage, screening of the amount of Pd NPs@LCpp required is the central aspect for deciding efficiency of the catalyst. In the present case, lowering the amount of catalyst from 15 wt% to 10 wt% to 8 wt% of the Pd NPs@LCpp could maintain the efficiency of the reaction (83-86%) (Table **4B.2**, entries **10-11**)**.** However, further lowering to 5 wt% caused a lowering in the yield to 76% (Table **4B.2**, entry **12**). The catalyst displayed its maximum efficiency at 50 °C (Table **4B.2, entry 10**) as lowering to 40 °C gave a relative reduction in the conversion yield (Table **4B.2**, entry **13**). Performing the reaction under N_2 atmosphere provided an interesting result. A drastic lowering in the yield to 58% is observed which suggests the role of air to re-oxidize a catalytic amount of reduced Ag(0) species to Ag(I) to attain complete reaction conversion with respect to the indole counterpart (Table **4B.2**, entry **14**). This result justifies the application of catalytic amount of Ag oxidant ample for achieving maximum performance with air as co-oxidant. In addition, reactions were performed in a variety of protic solvent media. Highest activity was observed in MeOH (Table **4B.2**, entry **2**) followed by EtOH which produced better results (Table **4B.2**, entry **15**) compared to PEG-300 where 58% conversion could be detected (Table **4B.2**, entry **16**). In pure H_2O, the present catalyst system could deliver only 40% of the desired transformation probably due to lower miscibility of indole (Table **4B.2**, entry **17**). When combination of solvents was tested, it was observed that a mixture of MeOH-H_2O (2:1) was unable to conclude any practical improvement in the system due to solubility issues (Table **4B.2**, entry **18**). However, when MeOH-H_2O (5:1) is used, arylation reaction reached to completion within 5 h with 91% yield of the C2-arylated product (Table **4B.2**, entry **19**). Thus, presence of a catalytic amount of water is found to accelerate the rate of reaction taking place in MeOH media. This acceleration could be related to the increased polarity of the solvent mixture [60]. As MeOH molecules when hydrogen

bonded to H_2O molecules are strongly polarized [60], which can interact with the boron centre more efficiently, thus facilitating the activation of arylboronic acid species in the reaction [61]. It is important to note that the present catalytic system holds complete regioselectivity and no significant isolable C3-arylation or homocoupling product could be detected. To further verify the practicality of the present catalyst over conventional homogeneous Pd catalysts, a reaction was performed using $Pd(OAc)_2$ which showed complete conversion in 8 h producing 82% of the major C2-product (Table **4B.2**, entry **20**). However, the multi-spot nature of the reaction also detected the homocoupling by-product and other side-products in the reaction media. Thus, highlighting the improved selectivity of the present catalyst system.

4B.2.4 Substrate Scope Study

Scope and limitations of the approach were therefore investigated by expanding the substrate scope to electronically diverse indole and arylboronic acid derivatives, as summarized in **Table 4B.3**. Almost every functionality in arylboronic acids participated in the regioselective arylation of 1-methylindole delivering C2-arylated products in successful results both in terms of yield and selectivity. The reaction is well tolerated by electron-rich substituents such as 2-methyl (Table **4B.3**, **3bb**) and electron-poor substituents such as 4-chloro, 3-nitro, 3-cyano groups (Table **4B.3**, **3bc-3be**), affording acceptable yields of C2-arylated products (78-87%). A combination of 1-methylindole and 2-naphthylboronic acid was assessed in the present system, showing 87% of the desired transformation in 5 h (Table **4B.3**, **3bf**). The protocol also showed acceptable results in the C2-arylation of indoles bearing different *N*-substituents. Besides 1-methylindole, indole nitrogen-bearing ethyl and benzyl groups proved their reactivity towards arylation and gave high yield (81-89%) and selectivity of the C2-arylated products (Table **4B.3**, **3bg-3bh**). However, when *N*-allyl indole was subjected in the current system an unusual result was observed, neither the reactant nor the arylated product could be traced after the reaction (Table **4B.3**, **3bi**). This might be possibly due to the coordination of Pd with the allylic double bond forming an η^2 alkene-Pd complex, thus failing to direct the reaction at C2 position.

Table 4B.3 Substrate scope for C2-arylation of indoles with arylboronic acids[a]

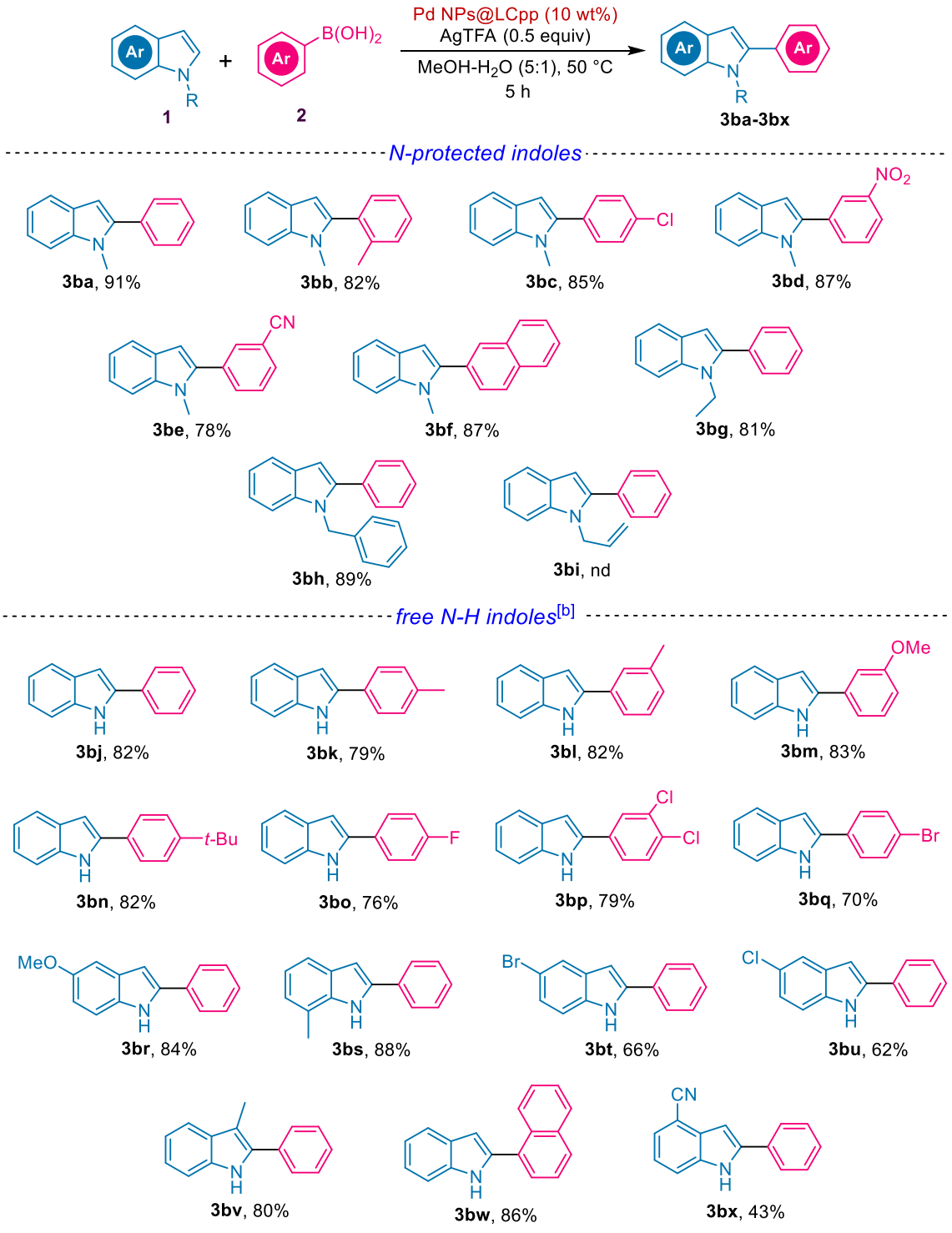

[a]Reaction conditions: **1** (1 mmol), **2** (1.2 mmol), Pd NPs@LCpp (10 wt%, 0.0015 mmol Pd), AgTFA (0.5 mmol), MeOH-H_2O 5:1 (2 mL), T (50 °C), time (5 h), in air; [b]reaction time (12 h); the yields reported are the isolated yields; nd (not detected).

Additional prospects into the present catalytic system were realized when arylation was attempted in indole rings bearing free *N*–H moiety. To our surprise, indole well

tolerated the system, giving the C2-arylated product in excellent isolated yield (82%) in 12 h (Table **4B.3**, **3bj**). This is a remarkable improvement of the present catalytic system compared to the methodology developed in Section **A**. Encouraged by the result, other combinations encompassing free *N*–H indole nucleus were also explored. C2-arylation of indole with arylboronic acids bearing electron-donating functionalities such as 4-methyl, 3-methyl, 3-methoxy, 4-*t*-butyl (Table **4B.3**, **3bk-3bn**), and electron-withdrawing functionalities such as 4-fluoro, 3,4-dichloro, 4-bromo moieties (Table **4B.3**, **3bo-3bq**), responded smoothly to the present system forming the desired arylation product in 70-83% yields. When 1-naphthylboronic acid was chosen as the arylating partner with indole, it produced the desired arylation in 86% yield (Table **4B.3**, **3bw**). Following, substituted indole ring derivatives bearing electron-donating groups such as 5-methoxy, 7-methyl were tested under the present system, where they gave 84% and 88% of product formation with phenylboronic acid respectively (Table **4B.3**, **3br-3bs**). However, indole rings bearing electron-withdrawing functionalities such as 5-bromo, 5-chloro, displayed relatively lowered reactivities yielding the desired products in 66% and 62% respectively (Table **4B.3**, **3bt-3bu**), and 4-cyanoindole could afford only 43% of the corresponding C2-arylated product (Table **4B.3**, **3bx**). Interestingly, steric demands of 3-methylindole did not disturb the reactivity and smoothly furnished 80% of the C2-arylated product (Table **4B.3**, **3bv**). It is noteworthy mentioning that no significant isolable C3 or C2,3-arylated side-product formation was observed and the reaction of free *N*–H and *N*-protected indoles obtained exclusively C2-arylated products without the installation of any directing groups or ligands to achieve site selectivity.

4B.2.5 Extension of Scope of the Reaction

Further scope and applicability of the developed catalyst system was evaluated in a sequential one-pot C2-functionalization followed by Suzuki-Miyaura coupling reaction. A molecule bearing bromo functionality was chosen as a substrate for the study, followed by a reaction conducted between 5-bromo-1-methylindole (**1**) and phenylboronic acid (**2a**) (Scheme **4B.1a**). A mild base, K_2CO_3 was added to the initial C2-arylated product **3ba´** (monitored by TLC) in the same reaction vessel without isolating the intermediate. After stirring for another 3 h, finally 1-methyl-2,5-

diphenylindole (**4a**) was formed *via* sequential one-pot double functionalization approach.

On a similar line (Scheme **4B.1b**), 1-methylindole (**1a**) was allowed to react with 4-bromophenylboronic acid (**2**), where the C2-arylated product **3bb´** was double functionalized to 2-([1,1'-biphenyl]-4-yl)-1-methylindole (**4b**) in one-pot following the process described above. Thus, the method extends introduction of additional functionalities in the indole heterocyclic core, thereby increasing their synthetic value. The Pd NPs@LCpp proved to be highly effective in both the steps of sequential transformations in a very low loading of Pd, avoiding any further addition to the subsequent step.

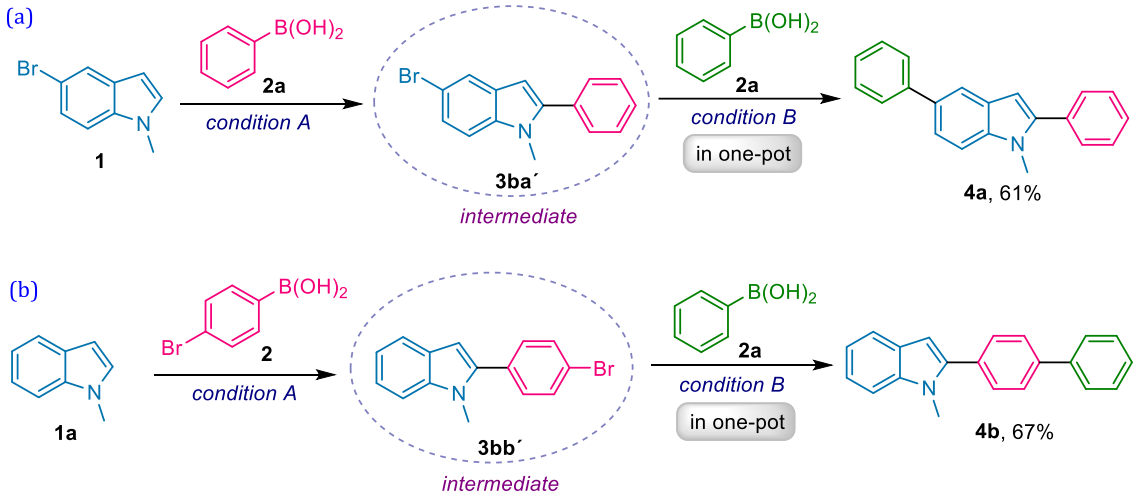

Reaction conditions: **A**: **1** (1 mmol), **2** (1.2 mmol), Pd NPs@LCpp (10 wt%), AgTFA (0.5 mmol), MeOH-H_2O 5:1 (2 mL), T (50 °C), time (5 h), in air; **B**: **2a** (1.2 mmol), K_2CO_3 (3 mmol), time (3 h); intermediate **3** detection through TLC monitoring.

Scheme 4B.1 Sequential one-pot double functionalization of indoles

4B.2.6 Recyclability Study

One crucial characteristic factor to justify the broader utility of a catalyst is the heterogeneity and recyclability studies. Therefore, the efficiency of the present catalyst towards reusability was assessed in C2-arylation of indoles. The model arylating substrates 1-methylindole (**1a**) with phenylboronic acid (**2a**) were allowed to react according to the optimized conditions (Table **4B.2**, entry **19**) for the study. As presented in Figure **4B.6**, the catalyst was found to be recyclable for at least five consecutive reaction cycles with product yield dropping to 80% after the 5th cycle.

This observed reduction in reactivity over the repeated use is probably due to partial blocking of some active sites and physical loss of the catalyst. An interesting observation was encountered during the reusability studies. In the first run 0.5 equiv Ag oxidant was added according to the optimization data producing 91% of the desired product. However, in the 2nd and subsequent reaction runs, it was found that even a catalytic amount of AgTFA oxidant is sufficient to complete the desired transformation with 80-91% yields.

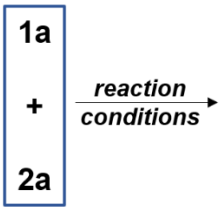

Cycle	1st run	2nd run	3rd run	4th run	5th run
Yield (%)	91	91	86	85	80
Oxidant (equiv)	0.5	0.3	0.2	0.2	0.2

Reaction conditions: **1a** (1 mmol), **2a** (1.2 mmol), Pd NPs@LCpp (10 wt%), MeOH-H_2O 5:1 (2mL), T (50 °C), time (5 h), in air.

Figure 4B.6 Reusability test for Pd NPs@LCpp

4B.2.7 Characterization of the Recovered Catalyst

To delve into the actual story for such an observation, the elemental profile and electronic information of the recovered catalyst was determined through XPS analysis. The high-resolution XPS spectrum of Pd 3d was obtained with four different binding energy peaks as shown in Figure **4B.7a**. Since the mechanism of C–H arylation of indoles is known to involve a classic Pd(0)↔Pd(II) catalytic cycle in presence of an oxidant. Thus, the high-resolution spectrum suggests higher concentration of Pd present as Pd(0) in the recovered catalyst than in the fresh Pd NPs@LCpp catalyst. Ag oxidant is used for this selective C2-arylation of indoles, which results in Ag(0) element found in the recovered catalyst during XPS analysis. Consequently, the high-resolution deconvoluted Ag 3d spectrum for recovered catalyst was obtained with two binding energy peaks at 366.9 eV and 372.9 eV, ascribed to the spin-orbit splitting of $3d_{5/2}$ and $3d_{3/2}$ of Ag(0), respectively (Figure **4B.7b**) [39].

The results from the reusability studies and the data obtained from XPS analysis of the recovered catalyst reveals some critical facts and information about the catalytic pathway. The detection of elemental Ag(0) in the re-used Pd NPs@LCpp can be

clearly attributed to the oxidizing ability of the Ag(I) salt, thus itself getting reduced during the reaction. Lignocellulose being an exceptional support material, efficiently adsorbs a considerable amount of the reduced Ag(0) particles into it. Henceforth, during the subsequent reaction runs using the re-used catalyst, the adsorbed Ag(0) particles are re-oxidized under the arial conditions thus allowing their participation as active species in the reaction. Thus, the method provides an additional advantage on curbing the amount of Ag oxidant due to the active participation of air as co-oxidant throughout the process.

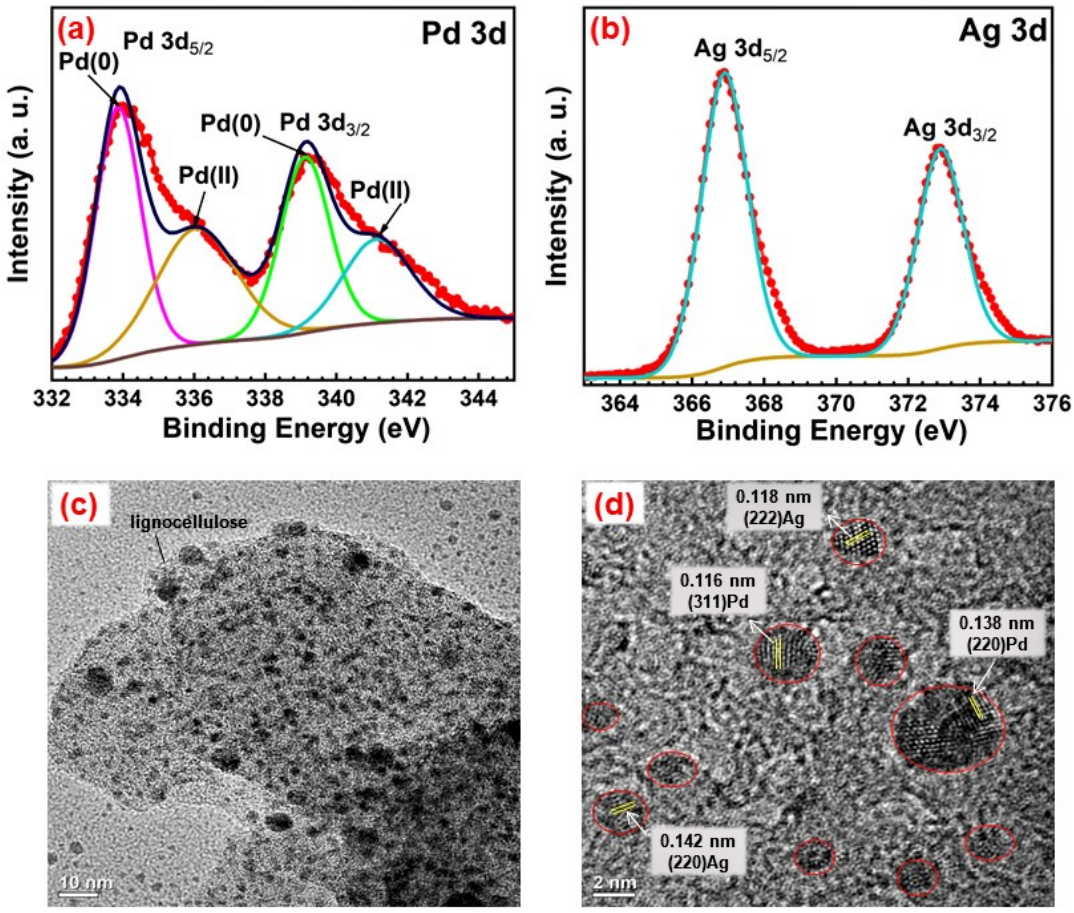

Figure 4B.7 High-resolution XPS spectra of (a) Pd 3d, and (b) Ag 3d, (c-d) TEM images of the recycled Pd NPs@LCpp catalyst

Furthermore, the TEM analysis on re-used Pd NPs@LCpp (Figure **4B.7c**) confirmed the adsorption of reduced Ag(0) species in the support, which is evident from the detection of lattice fingers with spacing 0.118 nm and 0.142 nm for (222) and (220) crystallographic planes of Ag respectively, along with the (311) and (220) planes of Pd(0) (Figure **4B.7d**).

4B.2.8 Nature of Active Catalyst Species

Finally, to gain more insight into the mode of Pd catalysis and the nature of active catalyst species involved in the catalytic cycle, a Pd level detection test was performed after the completion of reaction to detect any Pd leaching from the lignocellulose support. After the reaction of model arylating agents under the optimized condition (Table **4B.2**, entry **19**), the solid phase was filtered-off at the reaction temperature. The ICP-OES analysis of the liquid phase reveals a leached Pd level of less than 0.01 ppm. Thus, suggesting that no homogeneous active Pd species were present in the solution and so the reaction must have followed a plausible heterogeneous catalysis mechanism.

4B.2.9 Plausible Mechanism

From the literature, mechanism studies on Pd-catalyzed direct C2-arylation of indoles has well-established the initial electrophilic attack at C3 position of indole ring followed by a C3→C2 migration, as the most probable pathway for the selective C2-arylation (Scheme **4B.2**) [10,43]. In the present experimental system, the observation that no reaction proceeds in the absence of a Ag(I) oxidant (Table **4B.2**, entry **1**), suggests the initial generation of Pd(II) species (**II**) in presence of oxidant for the reaction to proceed. Now, Pd(II) species being relatively electrophilic than Pd(0), has the tendency to attack through the most electron-rich C3 position of the indole nucleus (**IV**). Also, the observation from substrate explorations that electron-rich indoles were more reactive towards the arylation than electron-deficient ones, clearly predicts the existence of electrophilic palladation-migration mechanism [42]. The subsequent reductive elimination forming C2-arylated indole (**VII**) with the regeneration of Pd(0) on the lignocellulose support, thus completes the catalytic cycle. Thus, the mechanism of the present reaction is expected to follow the similar catalytic pathway as proposed in Section **A**.

Although the mechanism involves Pd(II) species at the intermediate stages, the exceptional binding ability of lignocellulose material prevents Pd leaching from the support. This rationalizes our observations from heterogeneity and reusability studies of the catalyst and therefore improving the overall effectiveness of the newly developed Pd NPs@LCpp in directing-group-free C2-arylation of indoles.

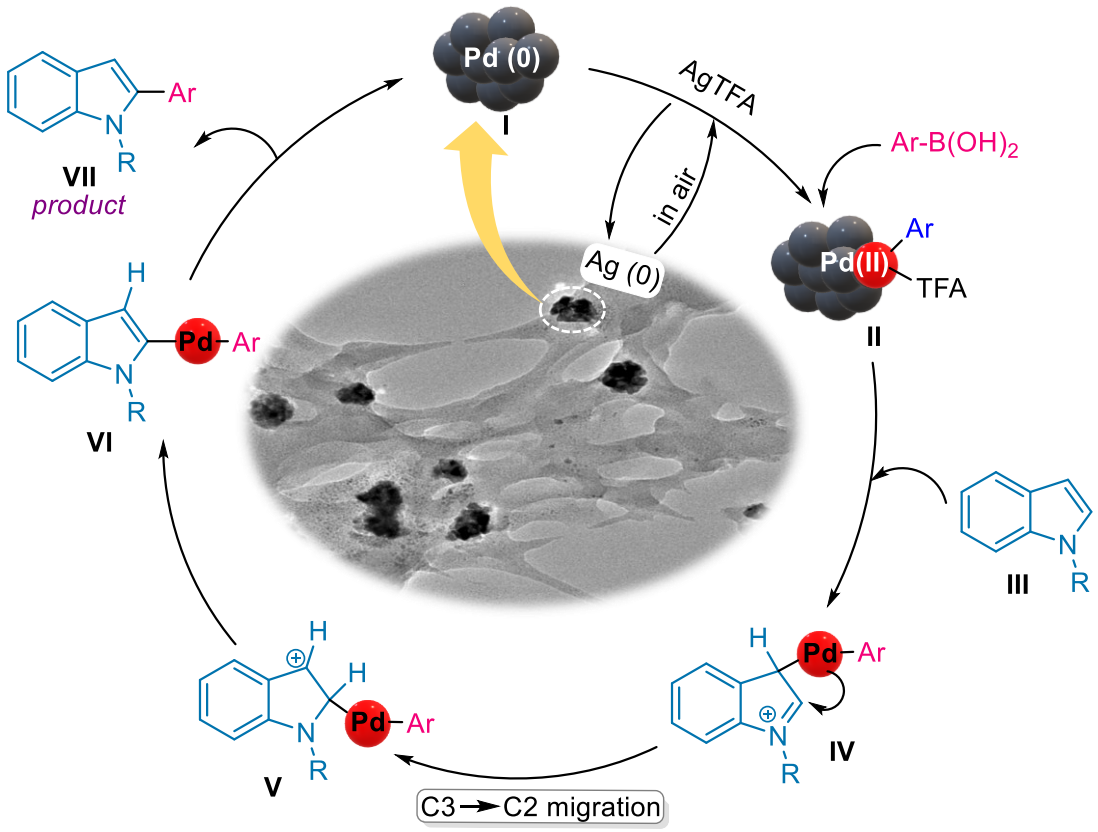

Scheme 4B.2 Plausible mechanism for C2-arylation of indoles with arylboronic acids

4B.3 Summary

This section demonstrated that lignocellulose derived from pomegranate peels can be utilized as a highly adaptable material for anchoring Pd nanoparticles, both in terms of its production route and material efficiency. The micrographs of lignocellulose-supported Pd nanomaterials showcase the synthesized Pd nanoparticles fairly entangled in the lignocellulose bio-support which stabilizes their dispersion. The synthesized Pd NPs@LCpp displayed remarkable catalytic efficiency in site-selective C2-arylation of *N*–H indoles with arylboronic acids without resorting to directing group installation on substrate.

Compared to Chapter **4** Section **A**, the catalyst developed in this section showed remarkable functionality tolerance towards indole bearing free *N*–H groups. The presence of lignocellulosic support offers multifunctional features over conventional Pd catalyst, in terms of improved activity, selectivity, free *N*–H functionality tolerance, minimal metal leaching, and reusability for at least five reaction cycles, thus improving the overall efficiency of the process. Optimization of the method revealed

the potential for minimizing Ag consumption throughout the re-cyclability course. The new catalyst was also found to be active for selective double functionalization of indole frameworks in a one-pot system. The sustainability profile presented by the process, unfolds a straightforward and scalable route to the production of raw biomass-based supported nanomaterials of high potentials.

4B.4 Experimental Section

4B.4.1 General Information

Reactions were carried out in Tarsons spinot digital magnetic stirrer and EYELA Process Station Personal Synthesizer PPS-CTRL1 under standard conditions. Analytical thin-layer chromatography (TLC) was carried out on Merck silica gel $60F_{254}$ plates using short wave (254 nm) and long wave (365 nm) UV light. Column chromatography purifications were performed over silica gel (100-200 mesh) and ethyl acetate/hexane as eluent. ^{1}H and ^{13}C NMR spectra were recorded on a JEOL JNM 400ECS NMR spectrometer (400 and 100 MHz respectively) using $CDCl_3$ as solvent and TMS as internal standard. The raw data of NMR were processed by MestReNova software. Chemical shifts (δ) are reported in ppm relative to the residual peak of the solvent ($CDCl_3$: ^{1}H NMR, δ = 7.25 ppm and sometimes δ = 1.56 ($CDCl_3$-water); and ^{13}C NMR, δ = 77.0 ppm) and TMS (0 ppm). Multiplicities are indicated as: s (singlet), d (doublet), t (triplet), q (quartet), m (multiplet), dd (doublet of doublets), dt (doublet of triplets) and br (broad). Coupling constants (J values) are given in hertz (Hz). All chemicals used were purchased commercially from either Sigma Aldrich, Merck or Alfa Aesar and used without further purification. Solvents used for extraction and chromatographic separations were distilled prior to use.

4B.4.2 Preparation of Catalysts

4B.4.2.1 ***Preparation of LCpp:*** 20 g waste peels of pomegranate fruit were collected, washed properly, finely crushed, ground, and mixed with 100 mL distilled water in a beaker. 10 mL of the aqueous peel suspension was taken in a centrifuge tube and rotated at 600 rpm. The white mass deposited in the bottom of the tube was washed 2-3 times with distilled water and dried under vacuum desiccator. The finely powdered white mass obtained was designated as LCpp.

4B.4.2.2 ***Preparation of Pd NPs@LCpp:*** 10 mL of the aqueous peel suspension was charged into a round-bottom flask, to which 50 mM (0.112 g) $Pd(OAc)_2$ was added at room temperature. The reaction mixture was stirred under N_2 atmosphere for 48 h. A change in the color from brown to black is indicative of the formation of Pd NPs. The resulting mixture was centrifuged (600 rpm) and washed with H_2O and dried under vacuum and finally crushed to fine black powdered Pd NPs@LCpp.

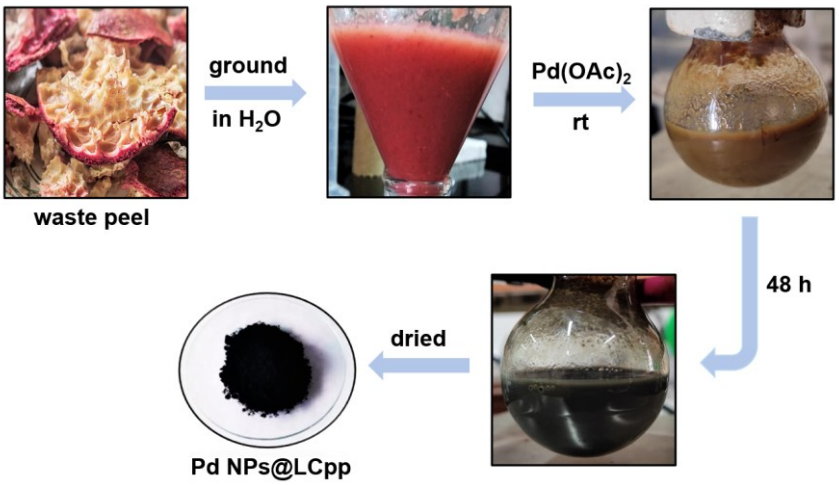

Figure 4B.8 Schematic preparation method of Pd NPs@LCpp from waste pomegranate peels

4B.4.3 Characterization of Catalysts

The powder XRD patterns were measured with the help of a Rigaku MultiFlex instrument using a nickel-filtered Cu K*α* radiation source operating at a wavelength of 0.154 nm. The surface structure and morphology of the catalyst were observed by SEM (model: JEOL JSM 6390 LV) and TEM (model: JEOL JEM 2100 at 200kV). The elemental composition of the catalyst was determined by EDX analysis using the same SEM instrument. XPS measurements were carried out using a Thermo-Scientific ESCALAB Xi+ spectrometer with a monochromatic Al Kα X-ray source (1486.6 eV) and a spherical energy analyzer that operates in the CAE mode. The CAE for the survey spectrum is 200 eV and for high-resolution spectra is 50 eV. FT-IR spectra were recorded on a PerkinElmer Frontier MIR/FIR spectrometer, the wavenumbers (ν) of recorded IR signals are reported in cm^{-1}. The real content of Pd was determined by ICP-OES analysis on an ACROS ICP spectrometer. BET surface area and porosity were measured, and the N_2 adsorption-desorption isotherms were recorded with a Quanta Chrome Novae-2200 surface area analyzer.

4B.4.4 Synthesis of *N*-Substituted Indoles

N-substituted indoles were prepared following the procedure discussed in Chapter **3**.

4B.4.5 General Procedure for C2-Arylation of Indoles with Arylboronic Acids

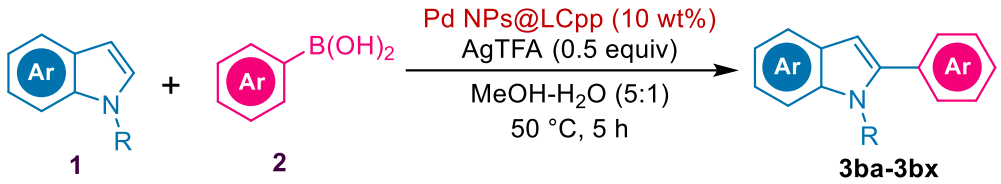

In a 50 mL round-bottom flask, a mixture of indole **1** (1 mmol) and arylboronic acid **2** (1.2 mmol), Pd NPs@ LCpp (10 wt%, 0.013 g) and AgTFA (0.5 mmol, 0.11 g) was stirred in MeOH-H_2O 5:1 (2 mL) solvent system at 50 °C for 5-12 h in air. Progress and completion of reaction was confirmed by TLC under short wave (254 nm) and long wave (365 nm) UV light. The reaction mixture was evaporated to remove the solvent MeOH, followed by extraction with ethyl acetate and water, dried over anhydrous Na_2SO_4 and concentrated under reduced pressure. The crude product was purified by column chromatography to give the corresponding C2-arylated products (**3ba**-**3bx**).

For ***reusability experiments***, the heterogeneous catalyst particles were recovered from the reaction media by centrifugation (600 rpm) and subsequently washed with water and ethyl acetate. The resultant catalyst particles were dried under vacuum and subjected to subsequent reaction runs.

4B.4.6 Procedure of One-Pot C2-Functionalization-Suzuki-Miyaura Coupling Reaction

To the C2-arylated product (**3ba´** and **3bb´**) obtained following the procedure discussed in section **4B.4.5**, K_2CO_3 (3 mmol) and arylboronic acid (1.2 mmol), were added in the same reaction flask (one-pot) and stirred for another 3 h. Progress and completion of reaction was confirmed by TLC in short wave (254 nm) and long wave (365 nm) UV light. The reaction mixture was evaporated to remove the solvent MeOH, followed by extraction with ethyl acetate and water, dried over anhydrous Na_2SO_4 and concentrated under reduced pressure. The crude product was purified by column chromatography to give the corresponding products **4a** and **4b** respectively.

4B.5 Characterization Data of the Products

1-Methyl-2-phenyl-1H-indole

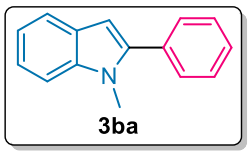

Obtained as white solid, 188 mg, 91% yield; ^{1}H NMR (400 MHz, $CDCl_3$), δ (ppm): 7.63 (d, J = 7.8 Hz, 1H), 7.52-7.43 (m, 4H), 7.40-7.34 (m, 2H), 7.24 (t, J = 7.3 Hz, 1H), 7.14 (t, J = 7.8 Hz, 1H), 6.56 (s, 1H), 3.73 (s, 3H); ^{13}C{^{1}H} NMR (100 MHz, $CDCl_3$), δ (ppm): 141.5, 138.3, 132.8, 129.4, 128.5, 127.9, 121.6, 120.5, 119.9, 109.5, 101.6, 99.9, 31.1.

1-Methyl-2-(o-tolyl)-1H-indole

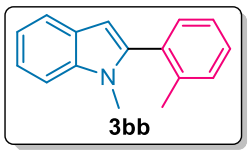

Obtained as white solid, 181 mg, 82% yield; ^{1}H NMR (400 MHz, $CDCl_3$), δ (ppm): 7.67 (dt, J = 7.9, 1.1 Hz, 1H), 7.39-7.26 (m, 6H), 7.20-7.16 (m, 1H), 6.59 (s, 1H), 3.78 (s, 3H), 2.47 (s, 3H); ^{13}C{^{1}H} NMR (100 MHz, $CDCl_3$), δ (ppm): 141.9, 138.4, 138.3, 132.9, 130.2, 128.8, 128.5, 128.1, 126.6, 121.7, 120.6, 119.9, 109.7, 101.6, 31.3, 21.7.

2-(4-Chlorophenyl)-1-methyl-1*H*-indole

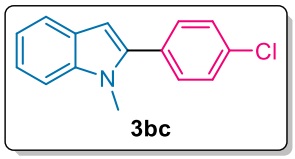

Obtained as yellow liquid, 205 mg, 85% yield; ^{1}H NMR (400 MHz, $CDCl_3$), δ (ppm): 7.63 (d, J = 7.8 Hz, 1H), 7.44 (s, 4H), 7.36 (d, J = 8.2 Hz, 1H), 7.28-7.24 (m, 1H), 7.15 (t, J = 6.9 Hz, 1H), 6.55 (s, 1H), 3.73 (s, 3H); ^{13}C{^{1}H} NMR (100 MHz, $CDCl_3$), δ (ppm): 140.2, 138.4, 134.0, 131.3, 130.5, 128.7, 127.8, 122.0, 120.6, 120.0, 109.6, 101.9, 31.2.

1-Methyl-2-(3-nitrophenyl)-1H-indole

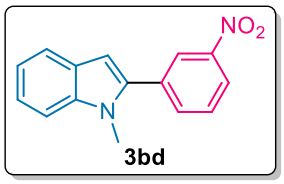

Obtained as yellow solid, 219 mg, 87% yield; ^{1}H NMR (400 MHz, $CDCl_3$), δ (ppm): 8.39 (t, J = 1.9 Hz, 1H), 8.27-8.24 (m, 1H), 7.85 (dt, J = 7.8, 1.4 Hz, 1H), 7.66 (t, J = 7.9 Hz, 2H), 7.40 (d, J = 8.2 Hz, 1H), 7.33-7.29 (m, 1H), 7.21-7.17 (m, 1H), 6.68 (s, 1H), 3.80 (s, 3H); ^{13}C{^{1}H} NMR (100 MHz, $CDCl_3$), δ (ppm): 148.3, 138.7, 138.6, 134.9, 134.5, 129.6, 127.6, 123.8, 122.6, 122.5, 120.9, 120.3, 109.8, 103.3, 31.3.

3-(1-Methyl-1H-indol-2-yl)benzonitrile

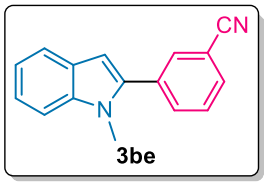

Obtained as white solid, 181 mg, 78% yield; ^{1}H NMR (400 MHz, $CDCl_3$), δ (ppm): 7.80 (t, J = 1.8 Hz, 1H), 7.74 (dt, J = 7.8, 1.6 Hz, 1H), 7.69-7.64 (m, 2H), 7.58 (t, J = 7.8 Hz, 1H), 7.38 (d, J = 8.3

Hz, 1H), 7.31-7.27 (m, 1H), 7.19-7.15 (m, 1H), 6.61 (d, *J* = 1.0 Hz, 1H), 3.75 (s, 3H); $^{13}C\{^{1}H\}$ NMR (100 MHz, $CDCl_3$), *δ* (ppm): 138.7, 134.2, 133.4, 132.5, 131.1, 129.4, 127.7, 122.5, 120.8, 120.3, 118.5, 112.9, 109.8, 103.0, 31.3.

1-Methyl-2-(naphthalen-2-yl)-1H-indole

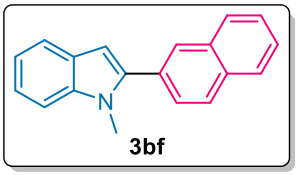

Obtained as white solid, 223 mg, 87% yield; ^{1}H NMR (400 MHz, $CDCl_3$), *δ* (ppm): 7.97-7.88 (m, 4H), 7.68-7.62 (m, 2H), 7.55-7.50 (m, 2H), 7.39 (d, *J* = 8.3 Hz, 1H), 7.29-7.25 (m, 1H), 7.18-7.14 (m, 1H), 6.67 (s, 1H), 3.81 (s, 3H); $^{13}C\{^{1}H\}$ NMR (100 MHz, $CDCl_3$), *δ* (ppm): 141.5, 138.5, 133.2, 132.7, 130.2, 128.3, 128.11, 128.08, 128.0, 127.8, 127.2, 126.5, 126.4, 121.8, 120.5, 119.9, 109.6, 102.1, 31.3 ppm.

1-Ethyl-2-phenyl-1H-indole

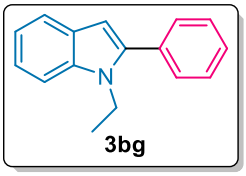

Obtained as colorless liquid, 179 mg, 81% yield; ^{1}H NMR (400 MHz, $CDCl_3$), *δ* (ppm): 7.64 (dd, *J* = 7.9, 1.1 Hz, 1H), 7.52-7.39 (m, 6H), 7.26-7.21 (m, 1H), 7.16-7.12 (m, 1H), 6.53 (s, 1H), 4.20 (q, *J* = 7.2 Hz, 2H), 1.32 (t, *J* = 7.2 Hz, 3H); $^{13}C\{^{1}H\}$ NMR (100 MHz, $CDCl_3$), *δ* (ppm): 141.1, 137.1, 133.2, 129.4, 128.5, 128.3, 128.0, 121.5, 120.5, 119.7, 109.9, 102.0, 38.7, 15.3.

1-Benzyl-2-phenyl-1H-indole

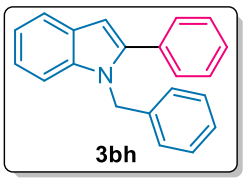

Obtained as colorless liquid, 252 mg, 89% yield; ^{1}H NMR (400 MHz, $CDCl_3$), *δ* (ppm): 7.70-7.67 (m, 1H), 7.47-7.45 (m, 2H), 7.42-7.37 (m, 3H), 7.32-7.24 (m, 3H), 7.21-7.14 (m, 3H), 7.05 (d, *J* = 6.5 Hz, 2H), 6.68 (s, 1H), 5.39 (s, 2H); $^{13}C\{^{1}H\}$ NMR (100 MHz, $CDCl_3$), *δ* (ppm): 142.0, 138.3, 138.1, 132.8, 129.4, 128.9, 128.7, 128.4, 128.2, 127.3, 126.1, 122.0, 120.7, 120.3, 110.7, 102.5, 47.8.

2-Phenyl-1H-indole

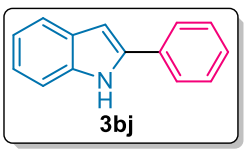

Obtained as white solid, 158 mg, 82% yield; ^{1}H NMR (400 MHz, $CDCl_3$), *δ* (ppm): 8.34 (br s, 1H), 7.68-7.61 (m, 3H), 7.46-7.39 (m, 3H), 7.34-7.30 (m, 1H), 7.21-7.17 (m, 1H), 7.14-7.10 (m, 1H), 6.83 (dd, *J* = 2.2, 1.0 Hz, 1H); $^{13}C\{^{1}H\}$ NMR (100 MHz, $CDCl_3$), *δ* (ppm): 137.9, 136.8, 132.4, 129.3, 129.0, 127.7, 125.2, 122.3, 120.7, 120.3, 110.9, 100.0.

2-(p-Tolyl)-1H-indole

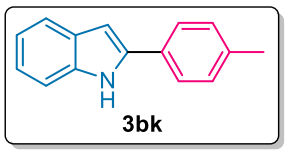

Obtained as white solid, 163 mg, 79% yield; ^{1}H NMR (400 MHz, $CDCl_3$), δ (ppm): 8.30 (br s, 1H), 7.61 (d, J = 7.8 Hz, 1H), 7.57-7.54 (m, 2H), 7.38 (d, J = 8.0 Hz, 1H), 7.26-7.24 (m, 2H), 7.20-7.16 (m, 1H), 7.13-7.09 (m, 1H), 6.78 (dd, J = 2.1, 1.0 Hz, 1H), 2.39 (s, 3H); ^{13}C{^{1}H} NMR (100 MHz, $CDCl_3$), δ (ppm): 138.0, 137.6, 136.7, 129.7, 129.6, 129.3, 125.0, 122.1, 120.5, 120.2, 110.8, 99.4, 21.2.

2-(m-Tolyl)-1H-indole

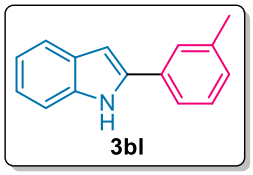

Obtained as white solid, 170 mg, 82% yield; ^{1}H NMR (400 MHz, $CDCl_3$), δ (ppm): 8.33 (br s, 1H), 7.62 (d, J = 7.9 Hz, 1H), 7.47 (d, J = 11.9 Hz, 2H), 7.39 (d, J = 7.0 Hz, 1H), 7.33 (t, J = 7.6 Hz, 1H), 7.20-7.09 (m, 3H), 6.81 (s, 1H), 2.42 (s, 3H); ^{13}C{^{1}H} NMR (100 MHz, $CDCl_3$), δ (ppm): 138.7, 138.0, 136.8, 132.3, 129.3, 128.9, 128.5, 125.9, 122.30, 122.25, 120.6, 120.2, 110.8, 99.9, 21.5.

2-(3-Methoxyphenyl)-1H-indole

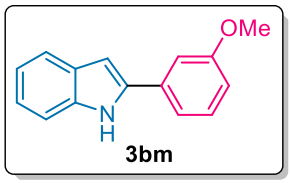

Obtained as colorless liquid, 185 mg, 83% yield; ^{1}H NMR (400 MHz, $CDCl_3$), δ (ppm): 8.33 (br s, 1H), 7.63 (d, J = 7.9 Hz, 1H), 7.40-7.34 (m, 2H), 7.26-7.18 (m, 3H), 7.12 (t, J = 6.9 Hz, 1H), 6.88 (dd, J = 8.3, 2.6 Hz, 1H), 6.82 (d, J = 2.3 Hz, 1H), 3.88 (s, 3H); ^{13}C{^{1}H} NMR (100 MHz, $CDCl_3$), δ (ppm): 160.1, 137.8, 136.8, 133.8, 130.1, 129.2, 122.4, 120.7, 120.3, 117.7, 113.1, 111.0, 110.9, 100.2, 55.4.

2-(4-(tert-Butyl)phenyl)-1H-indole

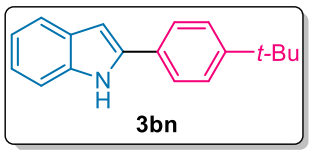

Obtained as white solid, 204 mg, 82% yield; ^{1}H NMR (400 MHz, $CDCl_3$), δ (ppm): 8.33 (br s, 1H), 7.63-7.59 (m, 3H), 7.48-7.45 (m, 2H), 7.40 (d, J = 8.0 Hz, 1H), 7.18 (t, J = 6.9 Hz, 1H), 7.11 (t, J = 6.9 Hz, 1H), 6.80 (dd, J = 2.3, 1.0 Hz, 1H), 1.36 (s, 9H); ^{13}C{^{1}H} NMR (100 MHz, $CDCl_3$), δ (ppm): 150.9, 138.0, 136.7, 129.6, 129.3, 126.0, 124.9, 122.1, 120.5, 120.2, 110.8, 99.5, 34.7, 31.3.

2-(4-Fluorophenyl)-1H-indole

Obtained as white solid, 160 mg, 76% yield; ^{1}H NMR (400 MHz, $CDCl_3$), δ (ppm): 8.28 (br s, 1H), 7.64-7.61 (m, 3H), 7.40 (d, J = 8.1 Hz, 1H), 7.20 (t, J = 6.9 Hz, 2H), 7.16-7.11

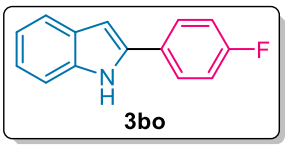

(m, 3H), 6.76 (dd, *J* = 2.3, 1.0 Hz, 1H); $^{13}C\{^{1}H\}$ NMR (100 MHz, $CDCl_3$), δ (ppm): 162.4 (d, *J* = 247.8 Hz), 137.0, 136.8, 129.2, 128.7, 126.9 (d, *J* = 8.0 Hz), 122.4, 120.6, 120.4, 116.1 (d, *J* = 21.8 Hz), 110.9, 99.9.

2-(3,4-Dichlorophenyl)-1H-indole

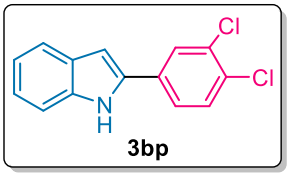

Obtained as white solid, 207 mg, 79% yield; ^{1}H NMR (400 MHz, $CDCl_3$), δ (ppm): 8.29 (br s, 1H), 7.73 (d, *J* = 1.4 Hz, 1H), 7.63 (d, *J* = 7.9 Hz, 1H), 7.51-7.46 (m, 2H), 7.40 (dd, *J* = 8.1, 1.0 Hz, 1H), 7.25-7.21 (m, 1H), 7.16-7.12 (m, 1H), 6.83 (dd, *J* = 2.1, 1.0 Hz, 1H); $^{13}C\{^{1}H\}$ NMR (100 MHz, $CDCl_3$), δ (ppm): 137.0, 135.3, 133.2, 132.4, 131.4, 131.0, 129.0, 126.7, 124.2, 123.1, 120.9, 120.6, 111.0, 101.3.

2-(4-Bromophenyl)-1H-indole

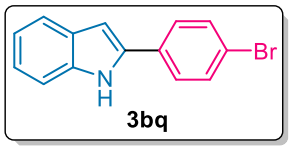

Obtained as white solid, 190 mg, 70% yield; ^{1}H NMR (400 MHz, $CDCl_3$), δ (ppm): 8.30 (br s, 1H), 7.63-7.50 (m, 5H), 7.39 (d, *J* = 8.1 Hz, 1H), 7.20 (t, *J* = 7.6 Hz, 1H), 7.12 (t, *J* = 6.9 Hz, 1H), 6.81 (d, *J* = 2.3 Hz, 1H); $^{13}C\{^{1}H\}$ NMR (100 MHz, $CDCl_3$), δ (ppm): 136.9, 136.7, 132.2, 131.4, 129.2, 126.6, 122.7, 121.5, 120.8, 120.5, 110.9, 100.6.

5-Methoxy-2-phenyl-1H-indole

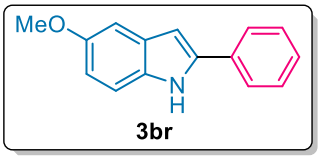

Obtained as white solid, 187 mg, 84% yield; ^{1}H NMR (400 MHz, $CDCl_3$), δ (ppm): 8.25 (br s, 1H), 7.62 (d, *J* = 7.9 Hz, 2H), 7.43-7.39 (m, 2H), 7.32-7.24 (m, 2H), 7.08 (d, *J* = 2.5 Hz, 1H), 6.85 (dd, *J* = 8.8, 2.5 Hz, 1H), 6.75 (d, *J* = 2.2 Hz, 1H), 3.85 (s, 3H); $^{13}C\{^{1}H\}$ NMR (100 MHz, $CDCl_3$), δ (ppm): 154.4, 138.6, 132.4, 132.0, 129.7, 129.0, 127.5, 125.1, 112.5, 111.7, 102.1, 99.8, 55.7.

7-Methyl-2-phenyl-1H-indole

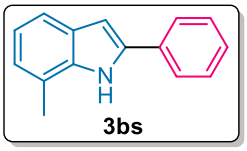

Obtained as white solid, 182 mg, 88% yield; ^{1}H NMR (400 MHz, $CDCl_3$), δ (ppm): 8.19 (br s, 1H), 7.71-7.68 (m, 2H), 7.50-7.43 (m, 3H), 7.33 (t, *J* = 7.4 Hz, 1H), 7.08-7.00 (m, 2H), 6.84 (d, *J* = 2.1 Hz, 1H), 2.55 (s, 3H); $^{13}C\{^{1}H\}$ NMR (100 MHz, $CDCl_3$), δ (ppm): 137.6, 136.4, 132.6, 129.0, 128.8, 127.6, 125.2, 122.9, 120.5, 120.02, 118.4, 100.6, 16.7.

5-Bromo-2-phenyl-1H-indole

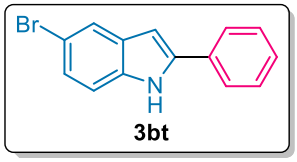

3bt

Obtained as white solid, 180 mg, 66% yield; ^{1}H NMR (400 MHz, $CDCl_3$), δ (ppm): 8.38 (br s, 1H), 7.74 (s, 1H), 7.64 (d, J = 7.1 Hz, 2H), 7.45 (t, J = 7.6 Hz, 2H), 7.37-7.34 (m, 1H), 7.26 (d, J = 1.4 Hz, 2H), 6.75 (d, J = 2.1 Hz, 1H); ^{13}C{^{1}H} NMR (100 MHz, $CDCl_3$), δ (ppm): 139.1, 135.4, 131.8, 131.0, 129.1, 128.1, 125.2, 125.1, 123.1, 113.4, 112.3, 99.4.

5-Chloro-2-phenyl-1H-indole

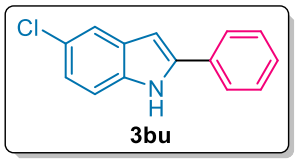

3bu

Obtained as white solid, 140 mg, 62% yield; ^{1}H NMR (400 MHz, $CDCl_3$), δ (ppm): 8.35 (br s, 1H), 7.65-7.63 (m, 2H), 7.58 (d, J = 2.1 Hz, 1H), 7.44 (t, J = 7.6 Hz, 2H), 7.36-7.29 (m, 2H), 7.13 (dd, J = 8.6, 2.0 Hz, 1H), 6.75 (d, J = 1.4 Hz, 1H); ^{13}C{^{1}H} NMR (100 MHz, $CDCl_3$), δ (ppm): 139.3, 135.1, 131.9, 130.3, 129.1, 128.1, 125.9, 125.2, 122.6, 120.0, 111.8, 99.6.

3-Methyl-2-phenyl-1H-indole

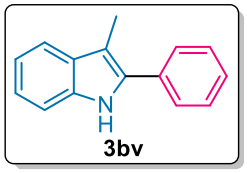

3bv

Obtained as colorless liquid, 165 mg, 80% yield; ^{1}H NMR (400 MHz, $CDCl_3$), δ (ppm): 8.03 (br s, 1H), 7.62-7.58 (m, 3H), 7.48 (t, J = 7.8 Hz, 2H), 7.38-7.36 (m, 2H), 7.23-7.19 (m, 1H), 7.17-7.13 (m, 1H), 2.46 (s, 3H); ^{13}C{^{1}H} NMR (100 MHz, $CDCl_3$), δ (ppm): 135.8, 134.0, 133.3, 130.0, 128.8, 127.7, 127.3, 122.3, 119.5, 119.0, 110.6, 108.7, 9.6.

2-(Naphthalen-1-yl)-1H-indole

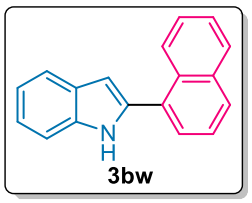

3bw

Obtained as colorless liquid, 210 mg, 86% yield; ^{1}H NMR (400 MHz, $CDCl_3$), δ (ppm): 8.34-8.32 (m, 2H), 7.95-7.89 (m, 2H), 7.72 (d, J = 7.9 Hz, 1H), 7.65 (dd, J = 7.1, 1.3 Hz, 1H), 7.57-7.50 (m, 3H), 7.46 (dd, J = 8.0, 1.0 Hz, 1H), 7.28-7.24 (m, 1H), 7.21-7.17 (m, 1H), 6.82 (dd, J = 2.2, 0.9 Hz, 1H); ^{13}C{^{1}H} NMR (100 MHz, $CDCl_3$), δ (ppm): 136.7, 136.4, 133.9, 131.6, 131.1, 128.9, 128.6, 128.5, 127.2, 126.7, 126.2, 125.7, 125.3, 122.2, 120.6, 120.2, 110.8, 103.7.

1-Methyl-2,5-diphenyl-1H-indole

Obtained as white solid, 172 mg, 61% yield; ^{1}H NMR (400 MHz, $CDCl_3$), δ (ppm): 7.85 (d, J = 1.7 Hz, 1H), 7.69-7.66 (m, 2H), 7.55-7.41 (m, 9H), 7.31 (t, J = 7.4 Hz, 1H), 6.61

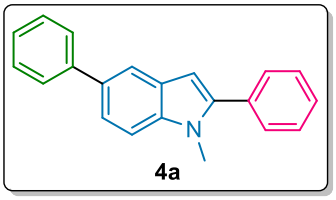

(s, 1H), 3.78 (s, 3H); $^{13}C\{^{1}H\}$ NMR (100 MHz, $CDCl_3$), δ (ppm): 142.6, 142.3, 137.9, 133.4, 132.7, 130.0, 129.3, 128.6, 128.4, 128.0, 127.4, 126.3, 121.5, 119.0, 110.0, 102.0, 31.4.

2-([1,1'-Biphenyl]-4-yl)-1-methyl-1H-indole

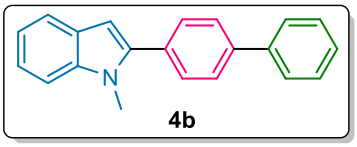

Obtained as white solid, 190 mg, 67% yield; ^{1}H NMR (400 MHz, $CDCl_3$), δ (ppm): 7.72-7.69 (m, 2H), 7.67-7.65 (m, 3H), 7.61-7.58 (m, 2H), 7.50-7.46 (m, 2H), 7.40-7.36 (m, 2H), 7.28-7.24 (m, 1H), 7.17-7.14 (m, 1H), 6.62 (d, J = 0.8 Hz, 1H), 3.80 (s, 3H); $^{13}C\{^{1}H\}$ NMR (100 MHz, $CDCl_3$), δ (ppm): 141.2, 140.6, 140.5, 138.5, 131.7, 129.7, 128.9, 128.0, 127.5, 127.2, 127.1, 121.8, 120.4, 119.8, 109.6, 101.8, 31.3.

4B.6 Representative ^{1}H and $^{13}C\{^{1}H\}$ NMR spectra

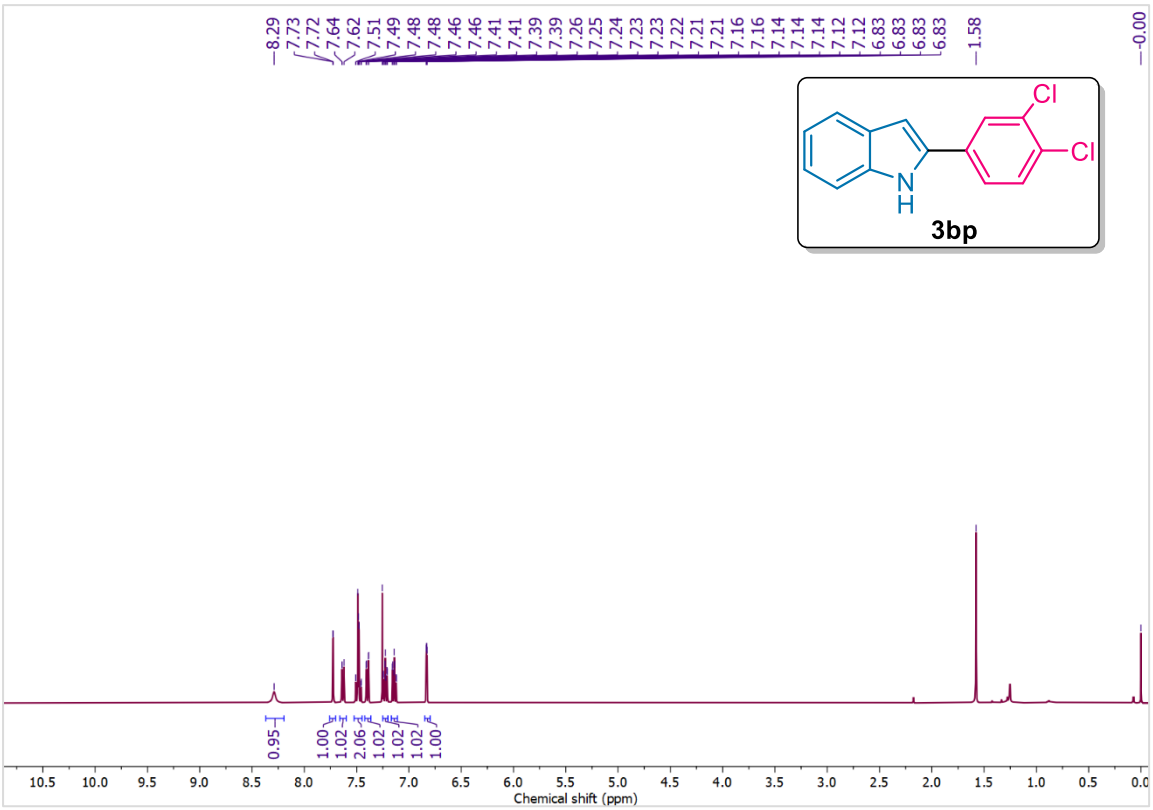

Figure 4B.9 ^{1}H NMR (400 MHz) spectrum of **3bp** in $CDCl_3$

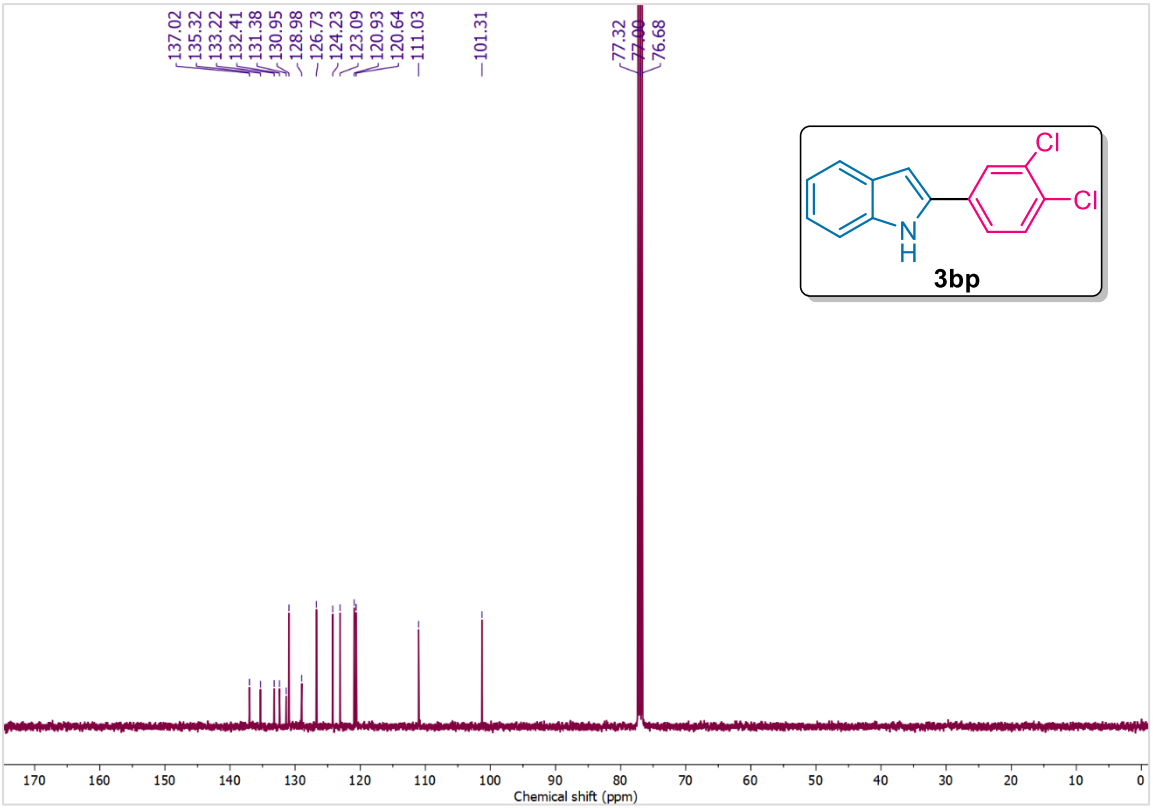

Figure 4B.10 $^{13}C\{^{1}H\}$ NMR (100 MHz) spectrum of **3bp** in $CDCl_3$

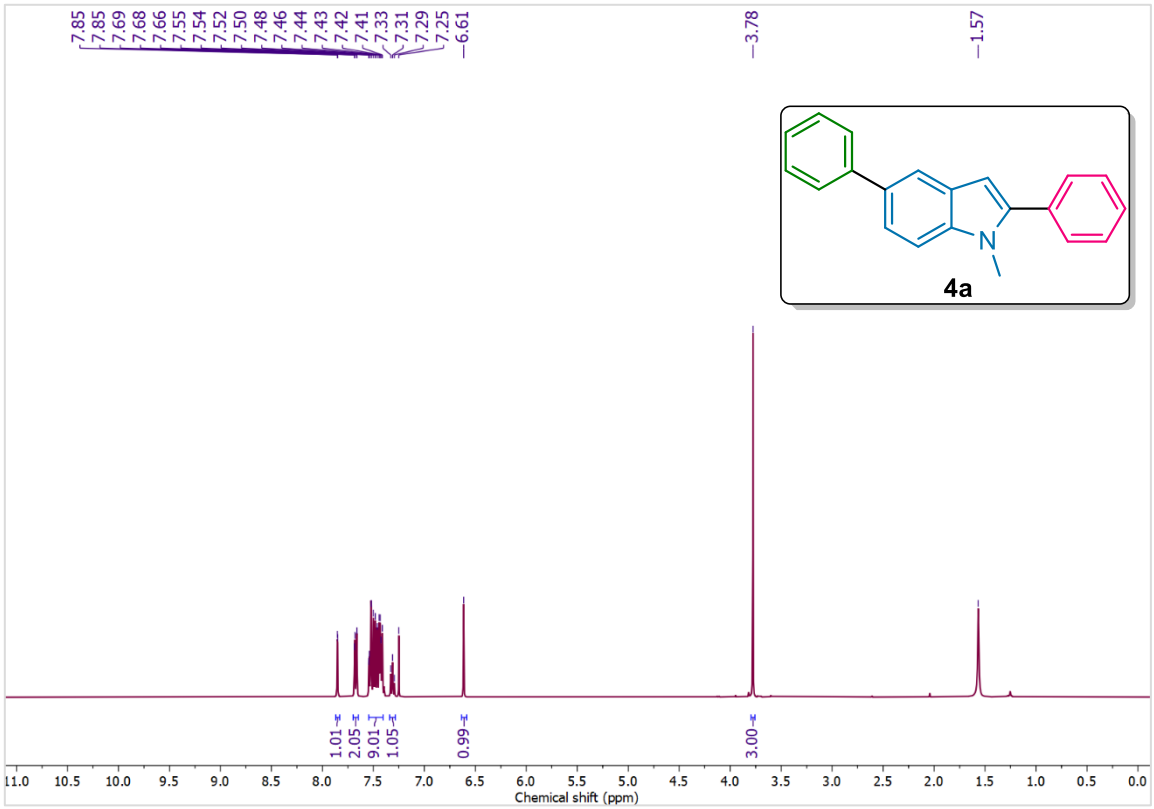

Figure 4B.11 ^{1}H NMR (400 MHz) spectrum of **4a** in $CDCl_3$

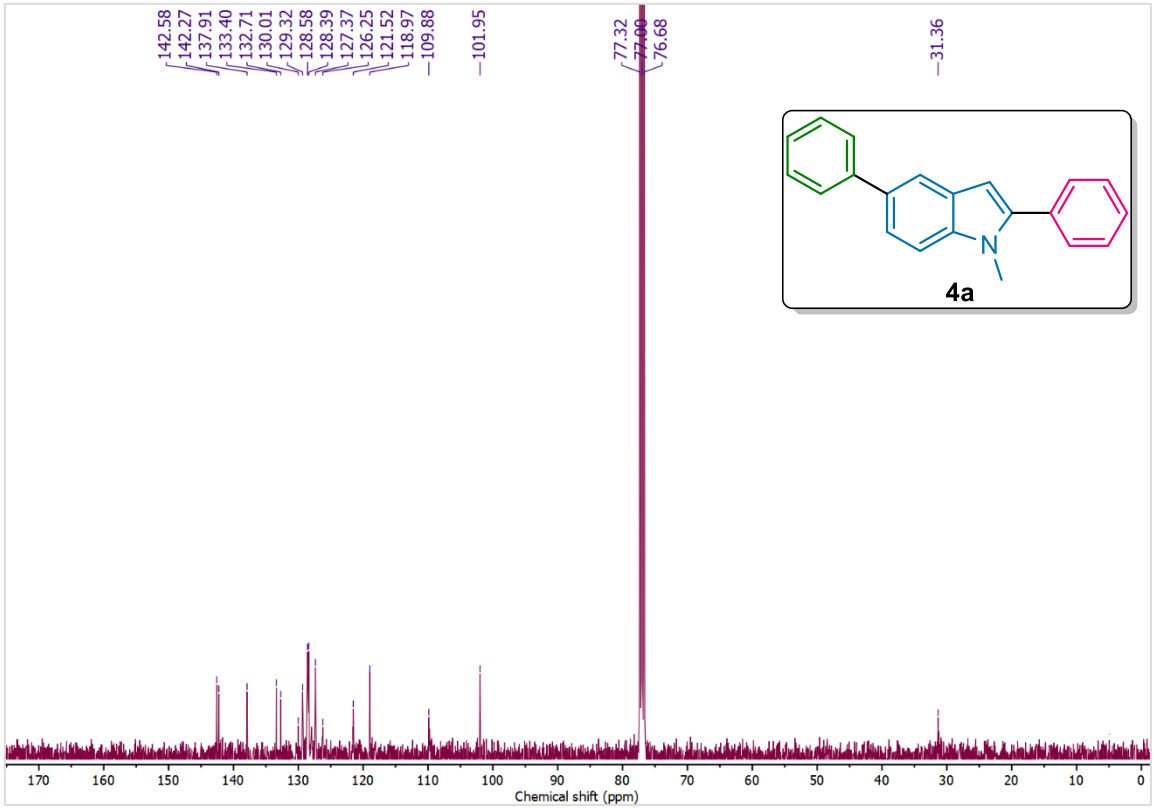

Figure 4B.12 $^{13}C\{^{1}H\}$ NMR (100 MHz) spectrum of **4a** in $CDCl_3$

4.1 Bibliography

[1] Urbina, K., Tresp, D., Sipps, K., and Szostak, M. Recent advances in metal catalyzed functionalization of indoles. *Advanced Synthesis & Catalysis*, 363(11):2723-2739, 2021.

[2] Gensch, T., Hopkinson, M. N., Glorius, F., and Wencel-Delord, J. Mild metal-catalyzed C–H activation: examples and concepts. *Chemical Society Reviews*, 45(10):2900-2936, 2016.

[3] Davies, H. M. and Morton, D. Recent advances in C–H functionalization. *The Journal of Organic Chemistry*, 81(2):343-350, 2016.

[4] Murugesan, T., Sivarajan, C., Jayakumari, C. M., Singh, R. K., Vennapusa, S. R., and Kaliyamoorthy, A. Palladium-catalyzed direct C2-biarylation of indoles. *The Journal of Organic Chemistry*, 86(15):10838-10851, 2021.

[5] Das, D., Bhutia, Z. T., Chatterjee, A., and Banerjee, M. Mechanochemical Pd(II)-catalyzed direct and C-2-selective arylation of indoles. *The Journal of Organic Chemistry*, 84(17):10764-10774, 2019.

[6] Konwar, D., Bora, P., Chetia, B., and Bora, U. Heterogeneous Pd/C-catalyzed ligand-free direct C-2 functionalization of indoles with aryl iodides. *ChemistrySelect*, 7(44):e202203009, 2022.

[7] Ghosh, M. K. and Rout, N. Aryl-aryl cross-coupling with hypervalent iodine reagents: aryl group transfer reactions. *ChemistrySelect*, 5(43):13644-13655, 2020.

[8] Budhwan, R., Yadav, S., and Murarka, S. Late stage functionalization of heterocycles using hypervalent iodine(III) reagents. *Organic & Biomolecular Chemistry*, 17(26):6326-6341, 2019.

[9] Hyatt, I. D., Dave, L., David, N., Kaur, K., Medard, M., and Mowdawalla, C. Hypervalent iodine reactions utilized in carbon–carbon bond formations. *Organic & Biomolecular Chemistry*, 17(34):7822-7848, 2019.

[10] Liang, Z., Yao, B., and Zhang, Y. $Pd(OAc)_2$-catalyzed regioselective arylation of indoles with arylsiloxane in acidic medium. *Organic Letters*, 12(14):3185-3187, 2010.

[11] Nareddy, P., Jordan, F., and Szostak, M. Ruthenium(II)-catalyzed direct C–H arylation of indoles with arylsilanes in water. *Organic Letters*, 20(2):341-344, 2018.

[12] Kumar, G. and Sekar, G. Pd-catalyzed direct C2-acylation and C2, C7-diacylation of indoles: pyrimidine as an easily removable C–H directing group. *RSC Advances*, 5(36):28292-28298, 2015.

[13] Zhang, J., Yao, L., Su, J. Y., Liu, Y. Z., Wang, Q., and Deng, W. P. Transition-metal-catalyzed aromatic C–H functionalization assisted by the phosphorus-containing directing groups. *Green Synthesis and Catalysis*, 2023. DOI: 10.1016/j.gresc.2023.02.001

[14] Chen, Z., Wang, B., Zhang, J., Yu, W., Liu, Z., and Zhang, Y. Transition metal-catalyzed C–H bond functionalizations by the use of diverse directing groups. *Organic Chemistry Frontiers*, 2(9):1107-1295, 2015.

[15] Sarkar, T., Shah, T. A., Maharana, P. K., Talukdar, K., Das, B. K., and Punniyamurthy, T. Transition-metal-catalyzed directing group assisted (hetero)aryl C–H functionalization: construction of C–C/C–heteroatom bonds. *The Chemical Record*, 21(12):3758-3778, 2021.

[16] Sun, C. L., Li, B. J., and Shi, Z. J. Pd-catalyzed oxidative coupling with organometallic reagents *via* C–H activation. *Chemical Communications*, 46(5):677-685, 2010.

[17] Basak, S. and Biswas, J. P. Transition-metal-catalyzed C–H arylation using organoboron reagents. *Synthesis*, 53(18):3151-3179, 2021.

[18] Wang, D., Salazar, C. A., and Stahl, S. S. Catalyst-controlled regioselectivity in Pd-catalyzed aerobic oxidative arylation of indoles. *Organometallics*, 40(14):2198-2203, 2021.

[19] Zhao, J., Zhang, Y., and Cheng, K. Palladium-catalyzed direct C-2 arylation of indoles with potassium aryltrifluoroborate salts. *The Journal of Organic Chemistry*, 73(18):7428-7431, 2008.

[20] Zheng, J., Zhang, Y., and Cui, S. Rh(III)-catalyzed selective coupling of *N*-methoxy-1*H*-indole-1-carboxamides and arylboronic acids. *Organic Letters*, 16(13):3560-3563, 2014.

[21] Yang, Z., Yu, J. T., and Pan, C. Recent advances in rhodium-catalyzed C(sp^2)–H (hetero)arylation. *Organic & Biomolecular Chemistry*, 19(39):8442-8465, 2021.

[22] Sollert, C., Devaraj, K., Orthaber, A., Gates, P. J., and Pilarski, L. T. Ru-catalyzed C–H arylation of indoles and pyrroles with boronic acids: scope and mechanistic studies. *Chemistry–A European Journal*, 21(14):5380-5386, 2015.

[23] Tiwari, V. K., Kamal, N., and Kapur, M. Ruthenium-catalyzed heteroatom-directed regioselective C–H arylation of indoles using a removable tether. *Organic Letters*, 17(7):1766-1769, 2015.

[24] Guo, X. X., Gu, D. W., Wu, Z., and Zhang, W. Copper-catalyzed C–H functionalization reactions: efficient synthesis of heterocycles. *Chemical Reviews*, 115(3):1622-1651, 2015.

[25] Aneeja, T., Neetha, M., Afsina, C. M. A., and Anilkumar, G. Progress and prospects in copper-catalyzed C–H functionalization. *RSC Advances*, 10(57):34429-34458, 2020.

[26] Zhu, X., Su, J. H., Du, C., Wang, Z. L., Ren, C. J., Niu, J. L., and Song, M. P. Cobalt(II)-catalyzed oxidative C–H arylation of indoles and boronic acids. *Organic Letters*, 19(3):596-599, 2017.

[27] Yang, S. D., Sun, C. L., Fang, Z., Li, B. J., Li, Y. Z., and Shi, Z. J. Palladium-catalyzed direct arylation of (hetero)arenes with arylboronic acids. *Angewandte Chemie*, 120(8):1495-1498, 2008.

[28] Campana, F., Massaccesi, B. M., Santoro, S., Piermatti, O., and Vaccaro, L. Polarclean/water as a safe and recoverable medium for selective C2-arylation of indoles catalyzed by Pd/C. *ACS Sustainable Chemistry & Engineering*, 8(44):16441-16450, 2020.

[29] Anastasiou, I., Van Velthoven, N., Tomarelli, E., Lombi, A., Lanari, D., Liu, P., Bals, S., De Vos, D. E., and Vaccaro, L. C2–H arylation of indoles catalyzed by palladium-containing metal organic framework in γ-valerolactone. *ChemSusChem*, 13(10):2786-2791, 2020.

[30] Duan, L., Fu, R., Zhang, B., Shi, W., Chen, S., and Wan, Y. An efficient reusable mesoporous solid-based Pd catalyst for selective C2 arylation of indoles in water. *ACS Catalysis*, 6(2):1062-1074, 2016.

[31] Huang, Y., Ma, T., Huang, P., Wu, D., Lin, Z., and Cao, R. Direct C–H bond arylation of indoles with arylboronic acids catalyzed by palladium nanoparticles encapsulated in mesoporous metal-organic-framework. *ChemCatChem*, 5(7):1877-1883, 2013.

[32] Malmgren, J., Nagendiran, A., Tai, C. W., Bäckvall, J. E., and Olofsson, B. C-2 selective arylation of indoles with heterogeneous nanopalladium and diaryliodonium salts. *Chemistry–A European Journal*, 20(42):13531-13535, 2014.

[33] Huang, Y., Lin, Z., and Cao, R. Palladium nanoparticles encapsulated in a metal–organic framework as efficient heterogeneous catalysts for direct C2 arylation of indoles. *Chemistry–A European Journal*, 17(45):12706-12712, 2011.

[34] Hegde, R. V., Ong, T. G., Ambre, R., Jadhav, A. H., Patil, S. A., and Dateer, R. B. Regioselective direct C2 arylation of indole, benzothiophene and benzofuran: utilization of reusable Pd NPs and NHC-Pd@ MNPs catalyst for C–H activation reaction. *Catalysis Letters*, 151:1397-1405, 2021.

[35] Eremin, D. B., Galushko, A. S., Boiko, D. A., Pentsak, E. O., Chistyakov, I. V., and Ananikov, V. P. Toward totally defined nanocatalysis: deep learning reveals the extraordinary activity of single Pd/C particles. *Journal of the American Chemical Society*, 144(13):6071-6079, 2022.

[36] Liu, S. Y., Li, H. Y., Shi, M. M., Jiang, H., Hu, X. L., Li, W. Q., Fu, L., and Chen, H. Z. Pd/C as a clean and effective heterogeneous catalyst for C–C couplings toward highly pure semiconducting polymers. *Macromolecules*, 45(22):9004-9009, 2012.

[37] Mao, Z., Gu, H., and Lin, X. Recent advances of Pd/C-catalyzed reactions. *Catalysts*, 11(9):1078, 2021.

[38] Kar, A. K., Kaur, S. P., Kumar, T. D., and Srivastava, R. Efficient hydrogenolysis of aryl ethers over Ce-MOF supported Pd NPs under mild conditions: mechanistic insight using density functional theoretical calculations. *Catalysis Science & Technology*, 10(20):6892-6901, 2020.

[39] Feng, J., Fan, D., Wang, Q., Ma, L., Wei, W., Xie, J., and Zhu, J. Facile synthesis silver nanoparticles on different xerogel supports as highly efficient catalysts for the reduction of *p*-nitrophenol. *Colloids and Surfaces A: Physicochemical and Engineering Aspects*, 520:743-756, 2017.

[40] Bay, K. L., Yang, Y. F., and Houk, K. N. Multiple roles of silver salts in palladium-catalyzed C–H activations. *Journal of Organometallic Chemistry*, 864:19-25, 2018.

[41] Lotz, M. D., Camasso, N. M., Canty, A. J., and Sanford, M. S. Role of silver salts in palladium-catalyzed arene and heteroarene C–H functionalization reactions. *Organometallics*, 36(1):165-171, 2017.

[42] Lane, B. S., Brown, M. A., and Sames, D. Direct palladium-catalyzed C-2 and C-3 arylation of indoles: a mechanistic rationale for regioselectivity. *Journal of the American Chemical Society*, 127(22):8050-8057, 2005.

[43] Grimster, N. P., Gauntlett, C., Godfrey, C. R., and Gaunt, M. J. Palladium-catalyzed intermolecular alkenylation of indoles by solvent-controlled regioselective C–H functionalization. *Angewandte Chemie International Edition*, 44(20):3125-3129, 2005.

[44] Shah, S. A., Ahmad, Z., Khan, S. A., Al-Ghamdi, Y. O., Bakhsh, E. M., Khan, N., ur Rehman, M., Jabli, M., and Khan, S. B. Biomass impregnated zero-valent Ag and Cu supported-catalyst: evaluation in the reduction of nitrophenol and discoloration of dyes in aqueous medium. *Journal of Organometallic Chemistry*, 938:121756, 2021.

[45] Kunwar, B., Deilami, S. D., Macaskie, L. E., Wood, J., Biller, P., and Sharma, B. K. Nanoparticles of Pd supported on bacterial biomass for hydroprocessing crude bio-oil. *Fuel*, 209:449-456, 2017.

[46] Akhtar, K., Ali, F., Sohni, S., Kamal, T., Asiri, A. M., Bakhsh, E. M., and Khan, S. B. Lignocellulosic biomass supported metal nanoparticles for the catalytic reduction of organic pollutants. *Environmental Science and Pollution Research*, 27:823-836, 2020.

[47] Isikgor, F. H. and Becer, C. R. Lignocellulosic biomass: a sustainable platform for the production of bio-based chemicals and polymers. *Polymer Chemistry*, 6(25):4497-4559, 2015.

[48] Yan, J., Oyedeji, O., Leal, J. H., Donohoe, B. S., Semelsberger, T. A., Li, C., Hoover, A. N., Webb, E., Bose, E. A., Zeng, Y., Williams, C. L., Schaller, K. D., Sun, N., Ray, A. E., and Tanjore, D. Characterizing variability in lignocellulosic biomass: a review. *ACS Sustainable Chemistry & Engineering*, 8(22):8059-8085, 2020.

[49] Fortunati, E., Yang, W., Luzi, F., Kenny, J., Torre, L., and Puglia, D. Lignocellulosic nanostructures as reinforcement in extruded and solvent casted polymeric nanocomposites: an overview. *European Polymer Journal*, 80:295-316, 2016.

[50] Yu, S., Sun, J., Shi, Y., Wang, Q., Wu, J., and Liu, J. Nanocellulose from various biomass wastes: Its preparation and potential usages towards the high value-added products. *Environmental Science and Ecotechnology*, 5:100077, 2021.

[51] Liao, Y., de Beeck, B. O., Thielemans, K., Ennaert, T., Snelders, J., Dusselier, M., Courtin, C. M., and Sels, B. F. The role of pretreatment in the catalytic valorization of cellulose. *Molecular Catalysis*, 487:110883, 2020.

[52] Hamawand, I., Seneweera, S., Kumarasinghe, P., and Bundschuh, J. Nanoparticle technology for separation of cellulose, hemicellulose and lignin nanoparticles from lignocellulose biomass: a short review. *Nano-Structures & Nano-Objects*, 24:100601, 2020.

[53] Pirzadeh, M., Caporaso, N., Rauf, A., Shariati, M. A., Yessimbekov, Z., Khan, M. U., Imran, M., Mubarak, M. S. Pomegranate as a source of bioactive constituents: a review on their characterization, properties and applications. *Critical Reviews in Food Science and Nutrition*, 61(6):982-999, 2021.

[54] Bar-Ya'akov, I., Tian, L., Amir, R., and Holland, D. Primary metabolites, anthocyanins, and hydrolyzable tannins in the pomegranate fruit. *Frontiers in Plant Science*, 10:620, 2019.

[55] Hasnaoui, N., Wathelet, B., and Jiménez-Araujo, A. Valorization of pomegranate peel from 12 cultivars: dietary fibre composition, antioxidant capacity and functional properties. *Food Chemistry*, 160:196-203, 2014.

[56] Sohni, S., Khan, S. A., Akhtar, K., Khan, S. B., Asiri, A. M., Hashim, R., and Omar, A. M. Room temperature preparation of lignocellulosic biomass supported heterostructure (Cu+Co@OPF) as highly efficient multifunctional nanocatalyst using wetness co-impregnation. *Colloids and Surfaces A: Physicochemical and Engineering Aspects*, 549:184-195, 2018.

[57] Lv, J., Wu, S., Tian, Z., Ye, Y., Liu, J., and Liang, C. Construction of PdO–Pd interfaces assisted by laser irradiation for enhanced electrocatalytic N_2 reduction reaction. *Journal of Materials Chemistry A*, 7(20):12627-12634, 2019.

[58] Lee, S. M., Lee, S. H., and Roh, J. S. Analysis of activation process of carbon black based on structural parameters obtained by XRD analysis. *Crystals*, 11(2):153, 2021.

[59] Anfar, Z., Ait Ahsaine, H., Zbair, M., Amedlous, A., Ait El Fakir, A., Jada, A., and El Alem, N. Recent trends on numerical investigations of response surface methodology for pollutants adsorption onto activated carbon materials: a review. *Critical Reviews in Environmental Science and Technology*, 50(10):1043-1084, 2020.

[60] Zhong, Y., Warren, G. L., and Patel, S. Thermodynamic and structural properties of methanol–water solutions using nonadditive interaction models. *Journal of Computational Chemistry*, 29(7):1142-1152, 2008.

[61] Hall, D. G. Boronic acid catalysis. *Chemical Society Reviews*, 48(13):3475-3496, 2019.